PCT WORLD INTELLECTUAL PROPERTY ORGANIZATION
International Bureau

INTERNATIONAL APPLICATION PUBLISHED UNDER THE PATENT COOPERATION TREATY (PCT)

(51) International Patent Classification 7 : G01N 21/00	A2	(11) International Publication Number: WO 00/43750
		(43) International Publication Date: 27 July 2000 (27.07.00)

(21) International Application Number: PCT/US00/01764

(22) International Filing Date: 25 January 2000 (25.01.00)

(30) Priority Data:
60/117,221 25 January 1999 (25.01.99) US

(71) Applicant *(for all designated States except US)*: NEWTON LABORATORIES, INC. [US/US]; Suite 4850, 800 West Cummings Park, Woburn, MA 01801 (US).

(72) Inventor; and
(75) Inventor/Applicant *(for US only)*: FULGHUM, Stephen, F. [US/US]; 9 Driftwood Road, Marblehead, MA 01945–1250 (US).

(74) Agents: HOOVER, Thomas, O. et al.; Hamilton, Brook, Smith & Reynolds, P.C., Two Militia Drive, Lexington, MA 02421 (US).

(81) Designated States: AE, AL, AM, AT, AU, AZ, BA, BB, BG, BR, BY, CA, CH, CN, CR, CU, CZ, DE, DK, DM, EE, ES, FI, GB, GD, GE, GH, GM, HR, HU, ID, IL, IN, IS, JP, KE, KG, KP, KR, KZ, LC, LK, LR, LS, LT, LU, LV, MA, MD, MG, MK, MN, MW, MX, NO, NZ, PL, PT, RO, RU, SD, SE, SG, SI, SK, SL, TJ, TM, TR, TT, TZ, UA, UG, US, UZ, VN, YU, ZA, ZW, ARIPO patent (GH, GM, KE, LS, MW, SD, SL, SZ, TZ, UG, ZW), Eurasian patent (AM, AZ, BY, KG, KZ, MD, RU, TJ, TM), European patent (AT, BE, CH, CY, DE, DK, ES, FI, FR, GB, GR, IE, IT, LU, MC, NL, PT, SE), OAPI patent (BF, BJ, CF, CG, CI, CM, GA, GN, GW, ML, MR, NE, SN, TD, TG).

Published
Without international search report and to be republished upon receipt of that report.

(54) Title: IMAGING OF TISSUE USING POLARIZED LIGHT

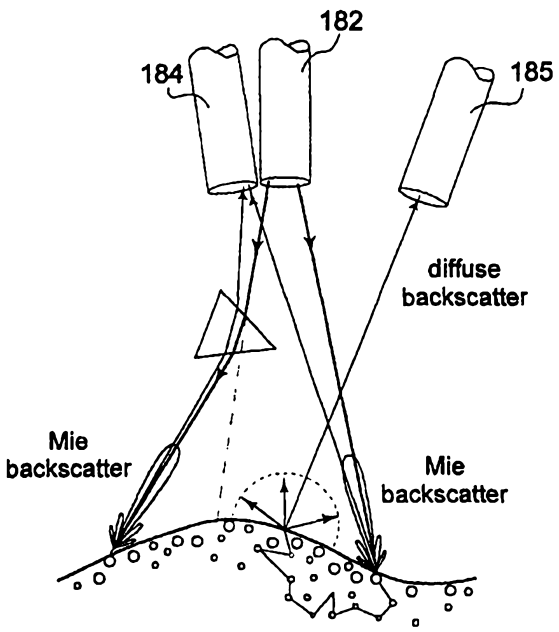

(57) Abstract

The present invention relates to the differential detection of directly backscattered light from epithelial tissues in order to determine the cell nuclear size distribution for the purpose of detecting tissue dysplasia. Light directly backscattered from surface tissue is differentiated from the light backscattered from underlying tissue by means of polarization, angular distribution or both. Both point measurement embodiments and imaging embodiments are presented. Optical systems for delivery and collection of light include endoscopic and fiber optic systems.

FOR THE PURPOSES OF INFORMATION ONLY

Codes used to identify States party to the PCT on the front pages of pamphlets publishing international applications under the PCT.

AL	Albania	**ES**	Spain	**LS**	Lesotho	**SI**	Slovenia
AM	Armenia	**FI**	Finland	**LT**	Lithuania	**SK**	Slovakia
AT	Austria	**FR**	France	**LU**	Luxembourg	**SN**	Senegal
AU	Australia	**GA**	Gabon	**LV**	Latvia	**SZ**	Swaziland
AZ	Azerbaijan	**GB**	United Kingdom	**MC**	Monaco	**TD**	Chad
BA	Bosnia and Herzegovina	**GE**	Georgia	**MD**	Republic of Moldova	**TG**	Togo
BB	Barbados	**GH**	Ghana	**MG**	Madagascar	**TJ**	Tajikistan
BE	Belgium	**GN**	Guinea	**MK**	The former Yugoslav Republic of Macedonia	**TM**	Turkmenistan
BF	Burkina Faso	**GR**	Greece			**TR**	Turkey
BG	Bulgaria	**HU**	Hungary	**ML**	Mali	**TT**	Trinidad and Tobago
BJ	Benin	**IE**	Ireland	**MN**	Mongolia	**UA**	Ukraine
BR	Brazil	**IL**	Israel	**MR**	Mauritania	**UG**	Uganda
BY	Belarus	**IS**	Iceland	**MW**	Malawi	**US**	United States of America
CA	Canada	**IT**	Italy	**MX**	Mexico	**UZ**	Uzbekistan
CF	Central African Republic	**JP**	Japan	**NE**	Niger	**VN**	Viet Nam
CG	Congo	**KE**	Kenya	**NL**	Netherlands	**YU**	Yugoslavia
CH	Switzerland	**KG**	Kyrgyzstan	**NO**	Norway	**ZW**	Zimbabwe
CI	Côte d'Ivoire	**KP**	Democratic People's Republic of Korea	**NZ**	New Zealand		
CM	Cameroon			**PL**	Poland		
CN	China	**KR**	Republic of Korea	**PT**	Portugal		
CU	Cuba	**KZ**	Kazakstan	**RO**	Romania		
CZ	Czech Republic	**LC**	Saint Lucia	**RU**	Russian Federation		
DE	Germany	**LI**	Liechtenstein	**SD**	Sudan		
DK	Denmark	**LK**	Sri Lanka	**SE**	Sweden		
EE	Estonia	**LR**	Liberia	**SG**	Singapore		

IMAGING OF TISSUE USING POLARIZED LIGHT

RELATED APPLICATIONS

This application claims the benefit of U.S. Provisional Application No. 60/117,221, filed on January 25, 1999, the contents of which the are incorporated herein by reference.

BACKGROUND OF THE INVENTION

More then 90% of cancer lesions are epithelial in origin. Several of the most common forms of epithelial cancers such as colorectal, esophageal, bladder, cervical and oral cancers have a well defined, detectable pre-cancer stage called dysplasia. Dysplasia is characterized by sequential accumulation of mutations in defined oncogenes and tumor suppresser genes. If detected, the absolute majority of the dysplastic lesions are curable. Clinical efforts to detect and treat this pre-cancerous stage of epithelial cancer have been shown to reduce the mortality rate.

Diagnosis of epithelial dysplasia remains difficult because it typically does not form macroscopic structures such as polyps, and is usually only visible after cancer has developed. Standard methods of detecting epithelial dysplasia are based on random biopsies and pathologic examination of the stained biopsy material. However, random biopsies have high sampling error. In many cases less than 1% of the epithelial surface at risk for dysplasia can be examined.

All types of epithelial dysplasia have several common characteristics, namely enlargement of epithelial cell nuclei with an increase in the nuclear to

cytoplasmic ratio, nuclear hyperchromatism, and increased number and stratification of epithelial cells. Despite these well-characterized epithelial changes, classification has been difficult as demonstrated by high inter-observer disagreement, even among experienced pathologists.

SUMMARY OF THE INVENTION

Non-invasive, *in-vivo* methods of detecting epithelial dysplasia provide for surveillance of epithelial surfaces, and the pathological diagnosis of pre-cancerous conditions in humans.

Optical techniques are well suited to be a substitution for random biopsies, since they are non-invasive, do not require tissue removal, and can be performed *in-vivo*. Moreover, they are fast (can be applied in real time), are relatively non-expensive, are able to work on microscopic scale, and thus can find very small dysplastic sites. The latter are highly likely to be missed by random biopsies.

The present invention relates to light scattering spectroscopy of polarized light to provide information about scatterers in surface layers of turbid media such as tissue. This process need not utilize fluorescence or absorption spectral features, but rather scattering properties of surface tissues such as epithelial layers. It can characterize properties of large scatterers (cell nuclei) in human epithelium and provide histological information about human tissues and diagnose dysplasia in real time in human organs *in-vivo*.

The idea of light scattering spectroscopy of unpolarized light to determine features of epithelial tissue has been described in U.S. Serial No. 08/948,734 filed on October 10, 1997, and in International Application No. PCT/US98/21450 filed on October 9, 1998, which designated the United States, the entire contents of these applications being incorporated herein by reference. The major centers of light scattering in epithelium are cellular organelles such as mitochondria and nuclei with the refractive index higher than that of the surrounding cytoplasm. Light backscattered from surface epithelial cell nuclei has an oscillatory wavelength dependent component. The periodicity of this component increases with nuclear

size, and its amplitude is related to the density of the nuclei. Thus, by analyzing the amplitude and frequency of the oscillatory component, the density and size distribution of epithelial nuclei can be determined. Normal nuclei have a characteristic diameter l=4-7 μm. In contrast, dysplastic nuclei can be as large as 20 μm. Nuclear size and density are important indicators of neoplastic precancerous changes in biological tissue. The ability to measure nuclear size distribution *in vivo* and in real time has valuable applications in clinical medicine. This enables the diagnosis of precancerous changes in various human organs such as esophagus, colon, bladder, oral cavity, cervix, etc. non-invasively and in-real-time.

Epithelium covers surfaces of organs in the human body. The thickness of epithelium ranges from 20 μm (one cell layer) to a few hundred microns (multiple cell layers). Beneath epithelium there are layers of relatively acellular connective and muscular tissues. Since dysplasia is limited to the epithelium, it is important to differentiate between the signal associated with the epithelium and underlying tissues. The backscattered component which carries information about surface epithelial nuclei is present in light reflected from mucosal tissues. However, it is ordinarily very small in amplitude, and easily masked by a background signal formed by diffuse scattering from the underlying tissue. To analyze that component the background signal must be removed. One can remove the diffuse background by modeling the general spectral features of the background. However, to make the approach more useful in practical medicine, and to be able to diagnose dysplasia *in vivo*, in real time, and in different organs, it is necessary to develop more robust method of removing or significantly reducing the diffuse component of the scattered light.

The present invention provides a method of measuring scattering features of epithelial cells by using polarized light spectroscopy. Note that initially polarized light loses its polarization while traveling through a turbid medium (tissue is an example of turbid medium). On the other hand the light scattered backward after a single scattering preserves polarization. Thus, by removing the nonpolarized component of the scattered light, one is able to distinguish light scattered by

epithelial cells. The residual spectrum can be further analyzed so that the size distribution of the nuclei and their density can be determined.

A preferred embodiment of the inventions includes a fiber optic light delivery and collection system for diagnoses of tissue. The fiber optic system can be housed in a probe housing proximal and distal ends where the distal end can be inserted into the various lumens of the human body for in vivo measurements of tissue. Polarizers can be used on the distal ends of both delivery and collection fibers. With optical fibers that preserve the polarization of light, the polarizers can be positioned at the proximal end of the probe. In a three fiber system, the probe can use a central delivery fiber and two off-center collection fibers that collect two different polarization components of light returning from the tissue. The polarizers can be birefringent crystalline materials such as quartz, sapphire or calcite. The calcite must be sealed from the working environment.

Another preferred embodiment of the invention includes imaging systems using polarized light to detect and image dysplasia. These systems can be used to image tissue samples or perform in vivo imaging of internal organs using endoscopic systems.

The direct backscatter signal from epithelial tissue, which carries the desired information on nuclear size distribution, and the diffuse backscatter signal, which must be removed before the size analysis, can be distinguished both by the polarization of the backscattered light and by its angular distribution. A preferred embodiment of a useful light scattering diagnostic takes advantage of both distinguishing characteristics. Such a diagnostic can be a point measurement, using fiberoptic probes, or an imaging diagnostic using lenses and spatial filters for angular differentiation as well as polarization-sensitive components for polarization differentiation. Preferred embodiments of both fiberoptic, point measurement systems and video imaging systems are described which are able to highlight areas of dysplastic tissue in vivo and in real time.

The wavelength dependence of light scattering from enlarged cell nuclei is the physical basis for applying light scattering spectroscopy to the detection of

dysplastic changes. The theory of the scattering of a plane electromagnetic wave from a transparent, homogeneous sphere was provided by Mie in 1908 and process has become known as Mie scattering. The theory shows that the intensity and the polarization of the scattered light varies with the angle at which it is scattered. The intensity and polarization distribution is determined by five parameters; the sphere diameter, the sphere's refractive index, the refractive index of the medium in which the sphere is embedded, the wavelength of the incident light in the medium and the polarization of the incident light. Generally normal nuclei can be represented as spheres with diameters of 5 to 7 μm and refractive indices of about 1.42, or generally in the range of 1.40 to 1.45, in a medium with a refractive index close to that of water (1.33). Dysplastic nuclei can be considered to be spheres with diameters of 10 μm and above.

Much of the diffusion of light through tissue is governed by the scattering of light from particles and in homogeneities which are smaller than a wavelength. This scattered intensity is uniform for all angles in the plane perpendicular to the plane of polarization of the light. In the plane of polarization, the scattered intensity forms two equal lobes in the forward and backward direction with no light scattered directly along the axis of polarization. For scattering sites with diameters of about one wavelength, the total scattered intensity is strongly peaked in the forward direction and the backscattered intensity is very small. The scattering from these relatively small sites dominates the scattered light which exits the tissue surface in the reverse direction after multiple scattering events deeper in the tissue. Such light has a very broad (diffuse) angular distribution and is essentially depolarized. Light exiting the tissue at a given point within an illuminated area of tissue is the sum of light scattered from all entrance points within that illuminated area so that polarization anisotropies in the individual scattering paths are averaged over all angles.

In contrast, scattering sites with diameters relatively large compared to the wavelength such as dysplastic nuclei, exhibit increasing backscattered intensity with increasing diameter. This backscattered intensity retains the

polarization of the incident light and is also sharply peaked with an angular distribution which is typically less than five degrees in width. Lobes in these backscattered angular distributions also shift direction and intensity with changes in the illuminating wavelength, giving rise to the spectroscopic signatures which are used to determine the diameter of the scattering site. Even though the absolute backscattered intensity is much smaller than the forward scattered intensity (it is typically smaller by a factor of 10^3) its narrow angle means that it can be efficiently collected by an optical fiber or imaging system, even when the optical aperture subtends a small solid angle. The collection efficiency of diffusely backscattered scattered light, for the same optical aperture, is significantly lower. Typically, only about 0.1% of the diffuse light is collected by a single optical fiber held a few millimeters from the tissue. In a properly designed light scattering spectroscopy probe, the backscatter signal can thus be equal to or stronger than the diffuse scatter signal.

The detailed designs of the fiberoptic, point-measurement systems and video imaging systems described below take advantage of these differences in angular distribution and polarization between the directly backscattered light carrying the desired information and the diffuse backscattered light which dilutes that signal. By performing differential measurements, based on polarization or angle or both, the desired signal can be extracted from the background, facilitating the analysis of nuclear size distribution in the epithelial tissue. The resulting diagnostic instruments are able to detect and/or image areas of dysplastic epithelium in vivo and in real time with out the need for the human-assisted analysis previously required.

BRIEF DESCRIPTION OF THE DRAWINGS

Figure 1 illustrates a preferred embodiment of a polarization-based light scattering spectroscopic system.

Figures 2 A and B are reflectance spectra of the two-layered tissue phantom (polystyrene beads on top of gel containing blood and $BaSO_4$) for parallel and perpendicular polarizations (notice characteristic hemoglobin dips) respectively.

Figures 3 A-D illustrate differences of two polarizations for (A) 4.56 μm beads in water (relative refractive index $n \approx 1.19$), (B) 9.5 μm beads in water ($n \approx 1.19$), (C) 5.7 μm beads in glycol ($n \approx 1.09$), (D) 8.9 μm beads in glycerol ($n \approx 1.07$) where the signals (dashed lines) are in good agreement with Mie calculations (solid lines) and the absorption features of hemoglobin are completely removed.

Figure 4 is a spectrum of the polarized (residual) component of back-scattered light: experimental data vs. fit of the Mie calculations for the polarized back-scattering for T84 cancerous colonic cells where best fits provide the following sets of parameters: average size 10.2 μm, standard deviation 1.5 μm, relative refractive index 1.045, and the sizes and standard deviations are in agreement with those measured using light microscopy.

Figure 5 is a spectrum of the polarized (residual) component of back-scattered light: experimental data vs. fit of the Mie calculations for the polarized back-scattering for normal intestinal cells where best fits provide the following sets of parameters: average size 5.0 μm, standard deviation 0.5 μm, relative refractive index 1.035, and the sizes and standard deviations are in agreement with those measured using light microscopy.

Figure 6 shows the nuclear size distribution for normal intestinal cells and T84 cancerous colonic cells where in each case, the solid line is the distribution extracted from the data, and the dashed line is the distribution measured using light microscopy.

Figure 7 schematically illustrates a fiber optic probe system for performing in vivo optical measurements of tissue in accordance with the invention.

Figures 8A and 8B show the distal end of a probe of a preferred embodiment of the invention.

Figures 9A-9C illustrate another preferred embodiment of a fiber optic probe in accordance with the invention.

Figures 10A-10C illustrate a preferred embodiment of a fiber optic probe device for delivery and collection of light.

Figures 11A-11D illustrate preferred embodiments of an imaging system in accordance with the invention.

Figure 12 is a cross-sectional view of a rigid probe imaging system in accordance with the invention.

Figure 13 illustrates a distal end of a probe imaging system in accordance with the invention.

Figure 14 is a cross-sectional end view of an imaging endoscope.

Figure 15 is a detailed cross-sectional view of a liquid crystal light valve to control illumination of the imaging sensor.

Figure 16 illustrates the resulting illumination of the imaging sensor.

Figure 17 illustrates a simple patient measurement probe.

Figure 18 illustrates another preferred embodiment of a probe tip.

Figure 19 illustrates another preferred embodiment of a probe tip in accordance with the invention.

Figure 20 illustrates a multifiber probe in accordance with the invention.

Figures 21A-21D illustrate features scattering measurements.

Figures 22A-B graphically illustrate results of scattering measurements.

The foregoing and other objects, features and advantages of the invention will be apparent from the following more particular description of preferred embodiments of the invention, as illustrated in the accompanying drawings in which like reference characters refer to the same parts throughout the different views. The drawings are not necessarily to scale, with emphasis being placed upon illustrating the principles of the invention.

DETAILED DESCRIPTION OF THE INVENTION

To determine properties of epithelial cells, one can correlate measured spectrum of the backscattered light with a model or representation. Using Mie theory, which provides the exact solution for the problem of light scattering by spherical objects of arbitrary sizes, the sizes and relative refractive indexes of the scatterers can be determined.

For polarized incident light, light scattered by a spherical particle with diameter d has components which are polarized parallel and perpendicular to the plane of scattering. For a plane polarized wave incident in direction $\hat{s}_0$, light scattered into direction $\hat{s}$ will have components which are polarized parallel (p) and perpendicular (s) to the plane of scattering. Intensities I_p and I_s of these components are related to the intensities of the incident light $I_p^{(0)}$ and $I_s^{(0)}$ as follows:

$$I_p(\hat{\mathbf{s}}) = 4\frac{\left|S_2(\hat{\mathbf{s}},\hat{\mathbf{s}}_0)\right|^2}{K^2d^2}\, I_p^o(\hat{\mathbf{s}}_0) \qquad (1)$$

$$I_s(\hat{\mathbf{s}}) = 4\frac{\left|S_2(\hat{\mathbf{s}},\hat{\mathbf{s}}_0)\right|^2}{K^2d^2}\, I_p^o(\hat{\mathbf{s}}_0) \qquad (2)$$

where k is the wavenumber of the incident light, S_1 and S_2 are scattering amplitudes which can be calculated numerically using Mie theory, and s_1 and s_2 are unit vectors defining propagation of the incident and scattered light. Scattering amplitudes are functions of a scattering angle $\vartheta = \cos^{-1}(\mathbf{s}\cdot\mathbf{s}_0)$ and are normalized so that integral $\int_0^{\pi}\left(\left|S_1(\vartheta)\right|^2 + \left|S_2(\vartheta)\right|^2\right)\sin\vartheta d\vartheta$ equals the total elastic scattering cross section.

Now consider an experiment in which linearly polarized incident light, intensity I_0, is distributed over solid angle $\Delta\Omega_0$ and scattering is collected over solid angle $\Delta\Omega$. The polarization, $\hat{\varepsilon}_0$, of the incident light can be decomposed into a component $\hat{\varepsilon}_p^o$, in the scattering plane (i.e. the plane formed by $\hat{s}$ and $\hat{s}_0$), and a perpendicular component $\hat{\varepsilon}_s^o$. By means of analyzers, we detect two orthogonal components of the scattered light intensity, $I_{\parallel}$ having polarization $\hat{\varepsilon}_a'$ and $I_{\perp}$ having

perpendicular polarization $\hat{\varepsilon}_a''$. The scattered intensity components are then given by

$$I_{\parallel} = \frac{2}{\pi k d^2} \int_{\Delta\Omega} d\hat{\mathbf{s}} \int_{\Delta\Omega} d\hat{\mathbf{s}}_0 I_0(\hat{\mathbf{s}}_0) \left| S_2(\hat{\mathbf{s}}_0, \hat{\mathbf{s}}) \cos\varphi \cos\varphi_0 + S_1(\hat{\mathbf{s}}_0, \hat{\mathbf{s}}) \sin\varphi \sin\varphi_0 \right|^2$$

(3)

$$I_{\perp} = \frac{2}{\pi k d^2} \int_{\Delta\Omega} d\hat{\mathbf{s}} \int_{\Delta\Omega} d\hat{\mathbf{s}}_0 I_0(\hat{\mathbf{s}}_0) \left| S_2(\hat{\mathbf{s}}_0, \hat{\mathbf{s}}) \cos\varphi \sin\varphi_0 - S_1(\hat{\mathbf{s}}_0, \hat{\mathbf{s}}) \sin\varphi \cos\varphi_0 \right|^2$$

(4)

If the incident light is completely collimated ($\Delta\Omega_0 = 0$), light scattered directly backward will be polarized parallel to the incident light polarization. In this case we can orient one of the analyzers parallel to the incident polarization direction ($\hat{\varepsilon}_0 \approx \hat{\varepsilon}_a'$). If the solid angles of the incident and collected light are sufficiently small and approximately equal, both $I_{\parallel}$ and $I_{\perp}$ will be present. However, the analyzer can still be positioned such that ($\hat{\varepsilon}_0 \approx \hat{\varepsilon}_a'$). Thus, in this case the collected light will still be highly polarized, and $I_{\parallel} >> I_{\perp}$. For this case the expression for the residual intensity, $I_{\parallel} - I_{\perp}$ can be simplified:

$$I_{\parallel} - I_{\perp} \approx \frac{4 I_0}{k d^2} \int_0^{\vartheta_0} \mathrm{Re}\left(S_1^*(\vartheta) S_2(\vartheta) \right) \sin\vartheta d\vartheta ,$$

(5)

with $\vartheta_0 = \sqrt{\frac{\Delta\Omega}{2\pi}}$.

Consider a system of two layers of scattering media such as epithelial tissue in which a thin layer of large scattered ($d >> \lambda$) covers a highly turbid layer of underlying tissue. Each of these layers gives rise to a different type of scattering. This two layer system represents optical properties of many human tissues with the first layer correlated with epithelium and second layer correlated with other tissue

layers beneath epithelium. The upper layer is optically thin so that it does not allow multiple scattering. Small portions of incident linearly polarized light is backscattered by the particles in the upper layer. The rest of the signal penetrates to the second layer that is optically thick. Light propagating through the second layer is randomized by means of multiple scattering. This diffusive light, if not absorbed in the second layer, returns to the surface. Thus, emerging light has two contributions: one from light backscattered by the particles of the first layer, I_b, and the other being diffusely reflected from the second layer, I_d. I_b has high degree of linear polarization that is parallel to the polarization of the incident light: $I_{\parallel}^{b} >> I_{\perp}^{b}$. As a result of multiple scatterings in the second layer, diffusely reflected light is depolarized and $I_{\parallel}^{d} = I_{\perp}^{d}$. Therefore, the residual intensity of the emerging light $I_{\parallel} - I_{\perp} \approx I_{\parallel}^{b} - I_{\perp}^{b}$ is dominated by the contribution from the upper layer and is substantially free from both absorption and scattering from the tissue below.

Expressions (3)-(5) relate $I_{\parallel} - I_{\perp}$ to the scattering amplitudes S_1 and S_2. The amplitudes depend on the wavelength of the light being scattered $\lambda = \pi/k$, the scatter's size d and the ratio of its refractive index to that of the surrounding medium, relative refractive index n. Therefore, the spectrum of the residual intensity varies with the scatterer's size and relative refractive index. Thus, sizes and refractive indexes of the scatterers can be found by fitting the representation of the Mie theory using equations (3)-(5) to the residual intensity spectrum.

A system 10 that measures excised tissue samples *in vitro* is illustrated in Figure 1. This system 10 delivers collimated polarized light on tissue 12 and separates two orthogonal polarizations of back-scattered light. The difference of these two components provides information about light scattered in the epithelial layer only. Since linearly polarized light is depolarized faster than circularly polarized light while passing through a random medium, linear polarization was used. The system provides light from a broadband source 14 (250 W tungsten lamp, Model 66181, Oriel Instruments, Inc., Stratford, CT) is collimated and then refocused with a small solid angle onto the sample using a fiber 16, a lens 18 and an aperture 20. A broadband polarizer 22 linearly polarizes the beam, before it is

delivered to the surface of a scattering medium through beamsplitter 24. The light beam strikes the surface of the sample with an angle ~15° relative to the normal in order to avoid specular reflectance. The diameter of the beam is 2mm. The reflected light is collected in a narrow cone (~0.015 radian) with apertures 26 and mirror 28 and two polarizations, parallel $I_{\|}$ and orthogonal $I_{\perp}$ to the initial polarization, are separated by a broadband polarizing beam splitter cube 28 which also acts as our analyzer (Melles Griot, Inc.). The output from this analyzer is delivered through lenses 30 and 200μm optical fibers 32, 34 (Ocean Optics, Inc., Dunedin, FL) into two channels of a multichannel spectroscope 36 (quadruple spectroscope, Model SQ200, Ocean Optics, Inc., Dunedin, FL). This enables the spectra of both components to be measured simultaneously in the range from 300 nm to 1200 or optionally in the range from 400 nm to 900 nm.

The beams are not perfectly collinear, and when they pass through the polarizer and analyzer cubes this gives rise to a small amount of distortion. Furthermore, the beamsplitter has different reflectivities for *s* and *p* polarizations. A diffusely reflective white surface was used as standard to correct for wavelength non-uniformity, and to calibrate the signals in the two channels. $I_{\perp}(\lambda)$ and $I_{\|}(\lambda)$ were each normalized to the corresponding background spectra, $I_{\perp}^{B}(\lambda)$ and $I_{\|}^{B}(\lambda)$ were each normalized to the corresponding background spectra, $I_{\|}^{B}(\lambda)$ and $I_{\perp}^{B}(\lambda)$ taken with the white diffusing surface. This removed spectral non-uniformities in the light source. Thus, the experiments actually measured the normalized residual intensity, ΔI:

$$\Delta I = \frac{I_{\|}}{I_{\|}^{B}} - \frac{I_{\perp}}{I_{\perp}^{B}}$$

(5)

Measurements on simple single- and two-layer systems were conducted to determine operational parameters. The single layer system included polystyrene beads of various sizes ranging from 0.5μm to 10μm (Polyscience, Inc.) embedded in

de-ionized water, glycol, or glycerol. The thickness of these layers was varied so that the optical thickness τ ranged from 0.1 to 5 a photon propagating through a medium with τ=1, undergoes one scattering event on average). The beads of large sizes 4-10 μm were used to represent cell nuclei. Since the relative refractive index of the polystyrene beads in water is about 1.2 (absolute refractive index is about n=1.59) and is substantially higher than that of the cell nuclei relative to the cytoplasm which is in the range from 1.03 to 1.1, glycol (n_a=1.45) and glycerol (n_a=1.48) were used instead of water to decrease the relative refractive index of the beads and, therefore, better approximate biological conditions.

In the single layer measurements the component of the backscattered light with the same state of polarization as the incoming light (denoted by $I_{\parallel}$) was almost 100 times larger than the component with the polarization orthogonal to the polarization of the incoming light (denoted by $I_{\perp}$). This establishes that single scattering from large spheroidal particles preserves polarization.

In the measurements with two layer models the first layer consisted of polystyrene beads embedded in water, glycol, or glycerol and was prepared as in the single layer measurements. The second layer included a gel containing solution of $BaSO_4$ powder which provided scattering properties of the second layer and human blood. Hemoglobin content of the blood provided absorptive properties to the model. This physical model simulated epithelium and underlying tissues. Adjusting concentrations of the $BaSO_4$ powder and blood, the scattering and absorption properties, can be made similar to those of a biological tissue, since in the optical spectral region hemoglobin is known to be the major absorber.

Figures 2A and 2B shows spectra of the parallel $I_{\parallel}$ and orthogonal $I_{\perp}$ polarized components of the light reflected from a two layer system. In this measurement, the first layer contained beads embedded in glycol. The beads had an average diameter of 4.56 μm. Standard deviation of their sizes was 0.03 μm. Optical thickness of the first layer was $\tau \sim 0.8$. The second layer was optically thick and its scattering and absorptive properties were comparable to those of a biological tissue. The spectrum of $I_{\perp}$ is dominated by characteristic hemoglobin absorption

bands. At the same time, characteristic spectral features of light scattered by 4.56 μm beads in the first layer, namely apparent ripple structure, and hemoglobin absorption in the second layer are seen in the spectrum of $I_{\parallel}$.

The residual spectrum ΔI is shown in Figure 3A. No hemoglobin absorption features are seen and the diffusive background coming from the second layer was completely removed. The ripple structure characteristic of scattering from spheres is evident. The comparison with Mie theory representation for scatterers with d = 4.56 μm , Δd=0.03μm and n=1.035 correspond with the μm shown in Figure 3B shows high degree of accuracy. The residual spectra obtained in measurements with other bead sizes (5.7μm, 8.9μm, and 9.5μm) embedded in any of the media used (water, glycol, and glycerol) had no measurable diffusive background component and agreed with Mie theory. Figure 3B shows the agreement between the theory and the measurements for 9.5 μm beads.

Similarly, the results of the measurements for 5.7 μm and 8.9 μm beads in glycerol and glycol are shown in Figures 3(C) and (D) respectively. Mie theory corresponds with the measured values in these cases as well. The high frequency ripple structure decreases as the relative refractive index gets smaller. The law frequency oscillations remain evident. Measurements showed that the instrument was able to detect signal from the bead solution of as low optical thickness as 0.05. Small disagreements seen in the spectrum can result from imperfect calibration of the instrument for the wavelength dependence of the optical elements used. The beams are not perfectly collinear and so there arises some imperfections in the polarized signals from the two channels when the beam passes through the polarizer and the analyzer elements. Further, the beam splitter used has different reflectivities for the *s* and the *p* polarized beams. However, using just a white standard, signals in the two channels were corrected for any wavelength non-uniformity and further used for calibration of signals.

Measurements with cell monolayers were conducted and the results are described in connection with Figures 4-6. A layer of gel containing solution of $BaSO_4$ powder and human blood under the monolayers is used to represent

underlying tissue. The concentrations of the $BaSO_4$ powder and blood, were adjusted to match optical properties of the biological tissue. Three types of cells were measured: normal intestinal cells, T84 cancer colonic cells and the fibroblasts. The measurements were similar to the measurements with beads. Nuclei of cells, however, had relative refractive indexes smaller then those of beads as well as larger size distributions which substantially eliminate the ripple structure. Fitting of the observed residual spectrum to Mie theory was performed. Three parameters in the fitting procedure were average size of the nuclei, standard deviation in size (a Gaussian size distribution was assumed), and relative refractive index.

For normal intestinal cells, the best fit was obtained using d=5.0μm,Δd=0.5μm, and n=1.045 (Figure 4). For the fibroblast cells, d-7.0 μm, Δd=1.0 μm and n=1.051 were obtained. For the T84 colon cancer cells the corresponding values were d=9.8 μm Δd=1.5 μm, and n=1.04 (Figure 5).

In order to check these results, the distribution of the average size of the cell nuclei was measured using light microscopy. The sizes and their standard deviations were in agreement with the parameters from Mie theory. A histogram showing the size distributions obtained for the normal T84 cells are shown in Figure 6. The accuracy of the average size is estimated to be 0.1 μm, and the accuracy in n as 0.001. Note the larger value of n obtained for cancerous cells, which is in agreement with the hyperchromaticity of cancer cell nuclei observed in conventional histopathology of stained tissue sections.

The backscattered signal can be described by Mie theory if the average size of the nuclei d, standard deviation in sizes Δd, and relative refractive index n are varied. Note that in Mie theory, dependence on d and n does not always come as a $(n-1)d$ product. Thus, the residual spectra have enough information to extract d and n simultaneously.

The size distributions for monolayers were compared to light microscopy and were in a good agreement for all three lines of cells. The accuracy of size and standard deviation extraction was approximately 0.1 μm which makes the method

useful in differentiating nuclei of different cell types, including cancerous and non-cancerous cells of the same organ.

Ability to detect cell nuclear enlargement and changes in refractive index of the nucleus (which can be related to the amount of DNA and protein in the nucleus) has valuable applications in clinical medicine.

The method of tissue diagnosis can be implemented either in a diagnostic device in which light can be delivered to points on the surface of the tissue, and collected and analyzed at each of those points on the surface of the tissue, and collected and analyzed at each of those points. In an *in vivo* system optical fibers are used to deliver and collect light. The fiber probe can be inserted in the endoscope biopsy channel or any similar device (depending on the type of the procedure and organ under study). Polarizer and analyzer can be placed at the tip of the probe in front of the delivery and collection fibers. Such an instrument can be used during routine endoscopic procedures to detect precancerous changes *in-vivo* in real time.

Such a probe system 40 is shown generally in Figure 7. This system 40 includes a broadband light source 42 that is optically coupled to a delivery fiber 44 extending through probe 50. As schematically shown in Figure 7, the probe 50 can be inserted through a channel in an endoscope 48, however the probe 50 can be constructed to be used separately. In a preferred embodiment described hereinafter, the light from source is directed through a polarizer at the distal end of probe 50. However, in another embodiment using polarization preserving optical fibers, a polarizer 26 can be used at the proximal end of probe fiber 44 to direct polarized light 46 through the fiber. Similarly, the proximal ends of collection fibers 65, 66 can employ polarizing elements 65, 66 respectively to transmit selected polarization components into the multichannel fiber spectrometer 54. The data can then be processed by computer 56, stored in computer 56, stored in computer memory and displayed on display 60 as needed.

The probe system can include a fiber optic probe having a distal end incorporating polarizers as seen in Figure 8A and 8B.

Figures 8A and 8B show the distal end of a probe 100 for the use of polarized light for in vivo diagnosis. Figure 8A shows a fiber optic device that is divided into three sections, the inner delivery fiber and two sets of collection fibers 150 and 152 that collect different polarization components. The cross-section of Figure 8B shows fibers 156 delivering light onto the tissue 140. They have to pass through a polarizer 120 which is also seen in the cross-section view of Figure 8B. The polarizing element is divided into at least two parts or elements 122, 126. Optical fibers 152 are arranged to collect the back reflected light from the tissue surface.

The backscattered light has two polarization components, corresponding to the parallel and the perpendicular components to the incident light. The two are differentiated by two different birefringent analyzers shown by two sectioned ring elements 122, 126. A first element 122 allows the parallel component to pass through while the second element 126 allows perpendicular component. A portion of element 122 polarizes light exiting fiber 156. As the fibers have low numerical apertures to collect light over very small angles, it is necessary to extend the distance 136 between the fiber ends and the aperture surface 142 opening to the tissue surface 140. It can be as long as 5mm. To avoid spurious internal reflections a glass block 130 is shown having refractive index n_2 lower than that of the shield 132 with refractive index n_1. The shield 132 can be coated with an absorbing element so that light hitting the boundaries is refracted out and then absorbed by the absorbing coating on the outer wall of the shield 132. The glass element 130 is beveled to avoid specular reflections from the tissue surface as it is described to increase the relative signal strength of the back-scattering. The light having the two orthogonal polarizations is separated and coupled to two spectrometer channels for detection and analysis.

Another preferred embodiment of a fiber optic probe 160 is illustrated in Figures 9A-9C. In this embodiment, delivery 156 and collection 162 fibers are housed in flexible tube 164 that is attached to a distal annular housing 166. Housing 166 includes a fiber retainer 106 and a polarizer 168 which can be a birefringent

crystal such as calcite, quartz or sapphire. Delivery fiber 156 delivers light from source 42 to polarizer 168 which delivers ordinary ray 170 through aperture 175 and window 178. Light returning through aperture 175 has ordinary 170 and extraordinary 172 components. The perpendicular component is collected by fibers 162 and the parallel component is collected by fibers 161. The delivery fiber 156 is positioned along the optical axis 176 of the crystal 168. Fibers 161, 156 are aligned along the aperture 175 of absorbing plate 178.

An improved method for this analysis involves performing a differential measurement of the backscattered light. Taking advantage of the fact that backward Mie scatter is differentiated by both angle and polarization from diffuse scatter. In this embodiment, a fiberoptic probe measures the backscattered light at two angles with a single polarization filter. By subtracting the two measured spectra the signal to noise ratio of the measurement is increased and the need to perform a parametric fit is eliminated.

Initially, since the original reflectance measurement technique required spectra for every point measurement, it seemed that an imaging device would be impractical. However, the use of polarized light for imaging can be provided using a system that generates a plurality of images at discrete wavelengths that detect different polarization and angular components.

The features of such an imaging system include an optical system which can take two images of the tissue, in a narrow wavelength band, that discriminates between the backscattered angle of the reflected light and the polarization of the reflected light. This accomplishes the differential measurement. These differential images are then acquired at as many different wavelengths as required to accomplish a final image which highlights areas of tissue with enlarged cell nuclei compared to normal cell nuclei.

The scattering of light by spheroidal particles as a function of angle and polarization is well described by Mie theory. Most incident light scattered from a cell nucleus continues generally in a forward direction. A small fraction, however, is backscattered within a narrow angle cone, with the same polarization as the

incident light. Generally, light scattered from large particles is more strongly peaked in the backwards direction than light scattered from smaller nuclei with a strength which has an oscillating dependence on the diameter of the cell nucleus relative to the wavelength of light. Analysis of this backscattered light, as a function of wavelength, provides a distribution of the density and diameter of the scattering particles as described above. Other types of scattered light, however, can dilute this backscattered light, making the analysis more difficult. Forward scattered light, after many repeated scattering events, may also exit the tissue in a generally backwards direction with a wide (diffuser) angular distribution. When a large area of tissue is illuminated with polarized light, as in the described imaging system, the diffused light exiting the tissue from any given point within the illuminated area has essentially no preferred polarization. This diffused light is the sum of light scattered to that point from all of the entrance points of the illuminated area. The polarization effects which can be seen on a single ray of light which has propagated through the tissue at a specific angle from the input polarization plane and a given distance from the entrance point are thus averaged out. This will be the case for all of the imaged points on the tissue surface as long as the illumination area extends sufficiently beyond the imaged area. The problem to be solved is the enhancement of the detection of the small quantity of directly backscattered light in the presence of the larger quantity of multiply scattered light.

The assembled view of Figures 9A and 9B show how the fibers are held together to maintain their relative angle. An appropriate sleeve 185 is placed around this assembly to protect the three long fibers 182, 184, 186 in the endoscope channel and to prevent direct light from entering the assembly from the side. The exploded view of the assembly in Figure 9C shows how the tip is assembled. The three fibers are surface glued (UV-curing polymer) onto a semi-cylindrical carrier which is molded from plastic with alignment grooves for the fibers. The cap semi-cylinder is glued on to hold them rigidly in place. The three fiber tips are then polished simultaneously so their surfaces are perpendicular to the carrier longitudinal axis. The carrier assembly is then optically glued to the end window.

Figure 22A shows that direct Mie backscatter from large particles can be collected more efficiently than diffuse backscatter from small particles by properly choosing the angular direction and collection solid angle of the receiving fiber. This improves the signal (direct backscatter) to noise (diffuse scatter) ratio. The tilt prevents direct reflections from the tip/tissue interface from getting into the receiving fibers.

These drawings assume that the direct backscatter is picked up by the same fiber that transmits the light to the tissue. Such single fiber designs have the virtue of lower costs for materials and assembly. The technical difficulty which must be overcome in their design is that surfaces perpendicular to the direction of the illumination beam in the optical train reflect some fraction of the light backwards into the detectors which are looking for tissue reflection. The design must thus avoid such surface reflections by tilting them at a sufficient angle to prevent such reflected light from propagating in the optical fiber. For typical fiber numerical apertures this requires a tilt of about 14 degrees. These single-fiber devices are shown in Figures 17 through 20.

The present embodiment of the invention accomplishes that enhancement by acquiring two, separate images of the tissue (in pairs, at multiple wavelengths, for example). Figure 11A shows a preferred embodiment of the imaging system that can be used for in vitro analysis or for exposed surface tissue. The optical train enhances the detection of the directly backscattered light in one image detected through lens 218 with image sensor 219 by passing only the light polarized parallel to the incident light, polarized light along with a spatial filter 217 at a focus in the optical train which passes only light within a narrow cone angle from the axis of the incident light. In this first image, some of the undesired light from diffuse, multiple-scatter events reaches the image. A second image detected with image sensor 223 receives light from lens 222 and spatial filter 221, also shown in Figure 11C, that blocks the passage of the directly backscattered light and passes only the off-axis light with a polarization perpendicular to the incident light. The images are recorded electronically with separate monochrome image sensor 219, 223 which can be

charge-coupled device (CCD) cameras. Electronically subtracting a fraction of the second image from the first image leads to a final image of the tissue which consists primarily of the directly backscattered light. This process is repeated at a sufficient number of wavelengths to allow the size of enlarged cell nuclei in the tissue to be differentiated from normal cell nuclei. This selection of wavelengths can be accomplished with a rotating filter wheel 204 shown in Figure 11B that is mounted on a rotating spindle 224 in front of a broadband light source 200, or by an electronically tuned liquid crystal filter in front of a broadband light source 200, or by a series of narrowband light sources combined onto one axis with a grating or scanning mirror. A lens 202 couples light from source 200 onto the filters 203 on wheel 204. A second lens 205 couples light exiting each filter 203 into a fiber 206, through aperture 207, prism 208 in optical coupler 209, lens 210, mirror 211, beamsplitter 212 and onto a tissue surface 213. Light returning from the tissue passes through beamsplitter 212, lens 214 and into optical coupler 209. The light returning from the tissue is either reflected by beamsplitter 215 onto mirror 220 and into filter 221 or is transmitted by beamsplitter 215 through aperture 216 and filter 217.

Alternatively, instead of elements 211, 212, another embodiment illustrated in Figure 11D uses mirror 228 and a nonpolarizing beamsplitter 226. This emobidment rduces the amount of back reflection occurancy in the embodiment fo Figure 11A. Beamsplitter 226 can also be used to replace element 215, for example, in system 209.

Shown in Figure 12 is a probe assembly 250 using a relay lens system in a distal section 254 that can be dimensioned appropriately for examinations of the oral cavity, cervix, or tissue exposed during laparoscopy. The proximal section 252 of probe 250 can employ the general design described in connection with Figure 11A.

Image sensors 270 and 272 collect images having different polarization components. The optical housing 280 includes mirror 282, beamsplitter 284, polarizing prism 285, polarizing beamsplitters 286, 288, spatial filters 266, 268, 290, and 292, delivery fiber 264, image reducing lens 274 and 276. Lens 260 and 262

can be spaced to form a telecentric optical coupling system. A window 258 can provide direct coupling to tissue surface 256.

Figure 13 shows a reflectance imaging system positioned in an endoscope tip that uses both differential polarization and differential angle. The arrangement shown in the top drawing only uses both differential polarization and differential angle. The arrangement shown in the top drawing only uses polarization as discussed below. The modified design shown at the bottom to the figure below the end-on view uses both polarization and angle to detect the direct Mie backscatter. Generally the liquid crystal switches work better in collimated light which favors the polarization only design, but they operate as shown in the polarization/angle design with some reduction of contrast. A further description regarding the use of twisted nematic, liquid crystal spatial light modulators is B.E.A. Saleh and M.C.Teich, *Fundamentals of Photonics, Wley, New York, NY, 1991,* pp 724-726, ISBN 0-471-83965-5, TA1520.S24, the contents of which is incorporated herein by reference.

Figure 13 shows an embodiment of an endoscope-based reflectance imaging system which enhances the detection of the direct Mie backscatter from cell nuclei with a polarization differentiation technique alone. The rigid endoscope tip, 300, is attached to the flexible section, 302, and capped with an end plug, 304. The end plug, shown in Figure 14 carries an imaging objective lens group, 306, along with the usual biopsy channel, 308, suction channel 310, and an auxiliary fiberoptic illumination port, 312, for normal, white light illumination of the tissue. The objective lens group, 306, images the tissue surface, 314, onto a CCD, video camera chip, 316, utilizing a second lens group, 318, which, along with 306, forms a telecentric imaging system. A non-polarizing, broadband beamsplitter, 320, couples illumination light onto the imaging axis. This illumination light comes from a small diameter optical fiber, 322, which is polarized by a transmission filter, 324. The diameter of the optical fiber, along with the focal length of the main objective lens group, 306, sets the angle subtended by the illumination onto the tissue for the reflectance measurement. A twisted, nematic, liquid-crystal cell, 328, is placed in the collimated beam after the lens group 318. A polarizer, crossed with respect to

the fiber optic polarizer, 324, is placed in front of the CCD camera where it is recorded as a digital image. This image is thus composed of the direct, Mie backscattered reflection (polarized) and half of the diffuse backscattered reflection from the tissue (unpolarized). When a longitudinal electric field is placed on the liquid crystal cell it passes both polarizations of the diffuse reflected light from the tissue and the direct Mie backscatter without rotating their polarizations. A second digital image is taken. In this image half of the diffuse reflected light passes through the polarizer, 330, and the direct Mie backscatter is blocked. Since the diffuse scatter is unpolarized, the two image components from the diffuse backscatter are identical. Taking the difference between the first image and the second image thus determines the direct Mie backscatter image alone. An iris placed at the focus of the telecentric lens system sets the angular extent of the reflected light which is passed for analysis.

A second embodiment shown in Figure 15 modifies the liquid crystal cell, 332, and its position in the imaging optical train. This allows the liquid crystal cell to block the direct Mie backscattered light both in terms of its polarization and angle. In this embodiment the cell is placed at the focus of the telecentric lens system so that it is sensitive to the angle of the imaging light rays. Only the central portion of the liquid crystal cell, 332, has an applied longitudinal voltage as shown in the orthogonal view of the liquid cell, 336 in Figure 16. In this embodiment, only the central rays, with the polarization of the illumination light, are blocked at the CCD camera. As before, two images are taken and their difference indicates the portion of the image due to direct Mie backscatter. The liquid crystal cell loses some of its ability to affect polarization at steep angles and practice may show that removing the lens elements, 338, to increase the focal length of the telecentric lens group may improve the image. This increases the overall length of the endoscope tip, however, which should be avoided if possible.

The same techniques of angle and polarization control can be used with single fiber point measuring reflectance probe as shown in Figures 17-20.

The optical system of Figure 17 launches the broadband light from source, 400, through an optical assembly, 402, into the fiber through a 50/50, non-polarizing beamsplitter, 404. This allows the return light from the tissue to pass through to the lens 406, which delivers it onto a detector or a spectrograph. A plate of absorbing glass, 408, is optically glued to the back surface of the beamsplitter assembly 404 to absorb the illumination light which is not directed to the fiber. The probe fiber tip is placed in a block 410, and the two are polished at the same angle as the beamsplitter assembly output face. The block thus keeps the fiber tip properly aligned to that face. A small drop of index matching fluid assists in reducing scatter from the fiber tip. Note that all of the surfaces through which the beam passes are tilted to avoid back reflections.

The single optical fiber, 412, carries the light to a probe tip, 415, which must provide, in general, a window 414 which holds the fiber tip at an offset from the tissue to allow the beam to expand somewhat and not present a puncture risk to the patient. The fiber tip in the probe is also held in a block 413 to facilitate polishing it at an angle. The tip of this window must also be tilted in window probe 417 shown in Figure 18 that provides two specific benefits. First, the negative lens, 416, shortens the length of the probe tip by making the tip of the transmit/receive fiber appear to be farther from the tissue surface. There is an optimal apparent optical distance for the received fiber tip from the tissue which maximizes the signal to noise ratio for a single fiber reflectance measurement. The negative lens provides this optical path in a shorter probe tip, allowing the tip to fit more easily through narrow, curved endoscope channels. The directly backscattered light is not significantly affected by this lens because it retraces its path back through the lens to the fiber tip from which the illumination came.

Probe 421 illustrated in Figure 19 shows that the optical element which accomplishes the redirection of the illumination does not have to be a common, spherical lens. The refracting surface in optical element 418 in distal end 421 is cone-shaped with an included angle which is less than 90 degrees to prevent a corner-cube reflection condition back into the transmit/receive fiber tip. This lens is

commercially available in broadband-transmitting sapphire at a very low price because this shape is used for jeweled pivot bearings. Note that there is no transmitted light which goes directly forward because of element 420 so that for this portion of the window, the amount of diffuse reflected light which makes it back into the transmit/receive fiber is also reduced.

Probe 425 illustrated in Figure 20 shows a preferred probe tip which also included the addition of a linear polarizing filter, 422, at the window tip. The directly backscattered light from the cell nuclei is polarized in the same plane as the illumination. The polarizing filter at the window tip absorbs all but one polarization of the illumination light and passes all of the directly backscattered light. The diffuse backscatter, however, is not polarized since it has undergone many out-of-plane scattering events which randomly rotates its polarization. Thus the diffuse backscattered light is reduced by a factor of two before it enters the transmit/receive fiber.

The additional received fibers, 424, shown in the preferred embodiment of probe 425 are aligned parallel to the central transmit/receive fiber to collect off-axis reflected light which is predominately due to the diffuse scattering processes. These fibers can be arranged in a circular ring around the central fiber and can be much narrower than the central fiber to maintain the flexibility of the total bundle. A fraction of the signal from these off-axis fibers can be subtracted from the signal from the central fiber to provide a differential measurement of the Mie direct backscattered light which carries the desired information on the tissue cell nuclei diameters. The appropriate subtraction factor can be measured by looking at tissue phantoms with very small scattering particles which only provide diffuse backscatter.

The high refractive index of sapphire allows the internal spaces 426 in the preferred probe between the tilted transmit/receive fiber tip and the sapphire window to be filled with a low-refractive-index fluid, such as water. This further reduces direct backscatter from the probe tip which might make it back to the detection system.

The graph of Figure 22B shows a result of a measurement of backscattered light from spherical particles in an index matching fluid illustrated generally in Figures 21A-D that the signal for either case of particle size is zero at zero distance because the overlap of the illumination and reception fiber view fields is zero. As the fibers pull back the overlap increases. At some point the $^1/r^2$ loss dominates and the signals stop increasing. With a further increase in distance the signal to noise increase. Eventually, however, the signal to noise drops due to the fixed noise inherent in the detection of the signal. The optimal position will be a distance where most of the large diameter backward scattering is collected but the $^1/r^2$ effect has not reduced the total signal to the point where it is comparable to thermal noise in the detectors. The apparent distance of the receiving fiber tip can be increased by using a negative lens at a short distance from the fiber tips, which could replace the usual plane window. This achieves the increase in signal to noise without requiring an 8 mm probe tip length. Figure 22B illustrates the results of differencing the two signals in Figure 22A.

While this invention has been particularly shown and described with references to preferred embodiments thereof, it will be understood by those skilled in the art that various changes in form and details may be made therein without departing from the spirit and scope of the invention as defined by the appended claims.

CLAIM

What is claimed is:

1. A method of imaging a region of interest comprising:
detecting polarized light from a region of interest; and
forming an image of the region of interest.

2. The method of Claim 1 further comprising collecting light from the region of interest with spatial filter.

3. The method of Claim 1 further comprising detecting a first image with a first image with a first detector and a second image with a second detector.

4. The method of Claim 1 further comprising providing an optical system that separates light from the region of interest along a first optical path an a second optical path.

5. The method of Claim 1 further comprising detecting a first polarization component and a second polarization component and process the detected components to provide an image of the region of interest.

6. A system for detecting abnormal tissue comprising:
a light source that directs light onto tissue;
a detector system that detects polarized light from the tissue to form an image of the tissue.

7. The system of Claim 6 wherein the detector system comprises a first detector and a second detector.

8. The system of Claim 7 further comprising an optical system that directs a first polarization component along a first optical path and that directs a second polarization component along a second optical path.

9. The system of Claim 6 further comprising a spatial filter that separates backscattered light along an optical axis from light backscattered within an angular range off the optical axis.

10. The system of Claim 6 further comprising a data processor that determines a size of cells within the tissue.

11. The system of Claim 6 further comprising a data processor that images epithelial dysplasia.

12. The system of Claim 6 wherein the light source comprises a broadband light source and a filer wheel.

13. The system of Claim 6 wherein the lightsource and detector system and optically coupled to tissue with an endoscope.

14. The system of Claim 6 further comprising a fiber optical probe that couples light from the light source onto the tissue.

15. The system of Claim 14 further comprising a delivery fiber and a collection fiber extending at a different angle than the delivery fiber.

16. The system of Claim 15 further comprising a second collection fiber extending at an angle different from the delivery and collection fibers.

17. The system of Claim 6 further comprising a data processor the subtracts a first image from a second image to provide a third image of abnormal tissue.

18. A system for detecting abnormal tissue comprising:

a light source that illuminates tissue.

an optical system that collects light from tissue at a plurality of angles;

determining a size of tissue cells from light collected at the plurality of angles.

19. The system of Claim 18 further comprising an analyzer that determines whether tissue cells are dysplastic, a detector system that detects backscattered light at the different angles, a fiber optic system that collects backscattered light and tissue fluorescence.

20. A method of imaging dysplasia comprising:

directing light onto tissue;

detecting backscattered light returning from the region of interest at different angles; and

forming an image of the tissue indicating regions which include epithelial dysplasia.

21. The method of Claim 20 further comprising the acquisition of a plurality of tissue images, each acquired by illumination with light at substantially different wavelengths.

22. The method of Claim 20 further comprising determining a size of tissue cells within the region imaged by means of the images acquired with different illumination wavelengths.

23. The method of Claim 20 further comprising directing illumination light onto the tissue with a restricted angular divergence.

24. The method of Claim 20 further comprising spatially filtering the backscattered light to allow separate imaging of the tissue with light backscattered within a restricted angle close to 180 degrees from the local illumination direction and with light diffusely backscattered at relatively large angles to the local illumination direction.

25. The method of Claim 20 further comprising the mathematical combination of two images acquired by means of the spatial filters of Claim 5 to produce an image derived predominately from light directly backscattered from near the surface of the epithelial tissue at angles close to 180 degrees from the local illumination direction.

26. The method of Claim 20 further comprising directing polarized illumination light onto the tissue.

27. The method of Claim 20 further comprising forming separate images of the tissue with backscattered light polarized parallel to the illumination polarization axis and perpendicular to the illumination polarization axis.

28. The method of Claim 20 further comprising the mathematical combination of two images formed with light of perpendicular polarizations to produce a single image derived predominately from light directly backscattered light polarized parallel to the illumination polarization axis.

29. The method of Claim 20 further comprising the formation of separate images of the tissue formed with backscattered light differentiated both by polarization and backscattered angle which are combined mathematically to

produce a single image of the tissue derived predominately from light directly backscattered from the tissue at an angle close to 180 degrees from the illumination direction and with a polarization parallel to the polarization of the illumination light.

30. A method of detecting epithelial tissue dysplasia comprising:

directing broadband, unpolarized light onto the tissue through an optical fiber and optical element;

detecting light directly backscattered from the tissue, through the optical element, within an acceptance angle relative to an illumination direction and in a plurality of wavelength bands including wavelengths from 300nm to 1200nm;

determining whether the illuminated tissue is normal or includes epithelial dysplasia.

31. A fiberoptic probe for measuring the directly backscattered light from the surface layer of tissue comprising;

an illumination fiber coupled to a broadband light source, the fiber delivering light onto the epithelial tissue through an optical element;

an optical element between the illumination fiber and the tissue to reduce a portion of diffusely backscattered light entering a detection optical fiber relative to a portion of directly backscattered light reaching the detection fiber;

a detection fiber to carry the predominately directly backscattered light to a detection system;

such that the a detection system determines the amount of light backscattered at a plurality of wavelengths relative to an amount of light directed to the tissue at the plurality of wavelengths.

32. The probe of Claim 31 in which the illumination fiber and the detection fiber are the same.

33. The probe of Claim 31 in which the optical element increases the divergence of the illumination light exiting the probe at the tissue surface.

34. The probe of Claim 31 in which the optical element polarizes both the light reaching the tissue from the illumination fiber and the backscattered light collected by the detection fiber.

35. The probe of Claim 31 in which a plurality of detection fibers are used, some of which are positioned to receive predominately light directly backscattered from the tissue at small angles to the illumination axis at the tissue surface and some of which are positioned to receive light backscattered at larger angles to the illumination axis, the detection system differentiating backscattered components to determine the amount of light at each detection wavelength which is directly backscattered from the tissue surface.

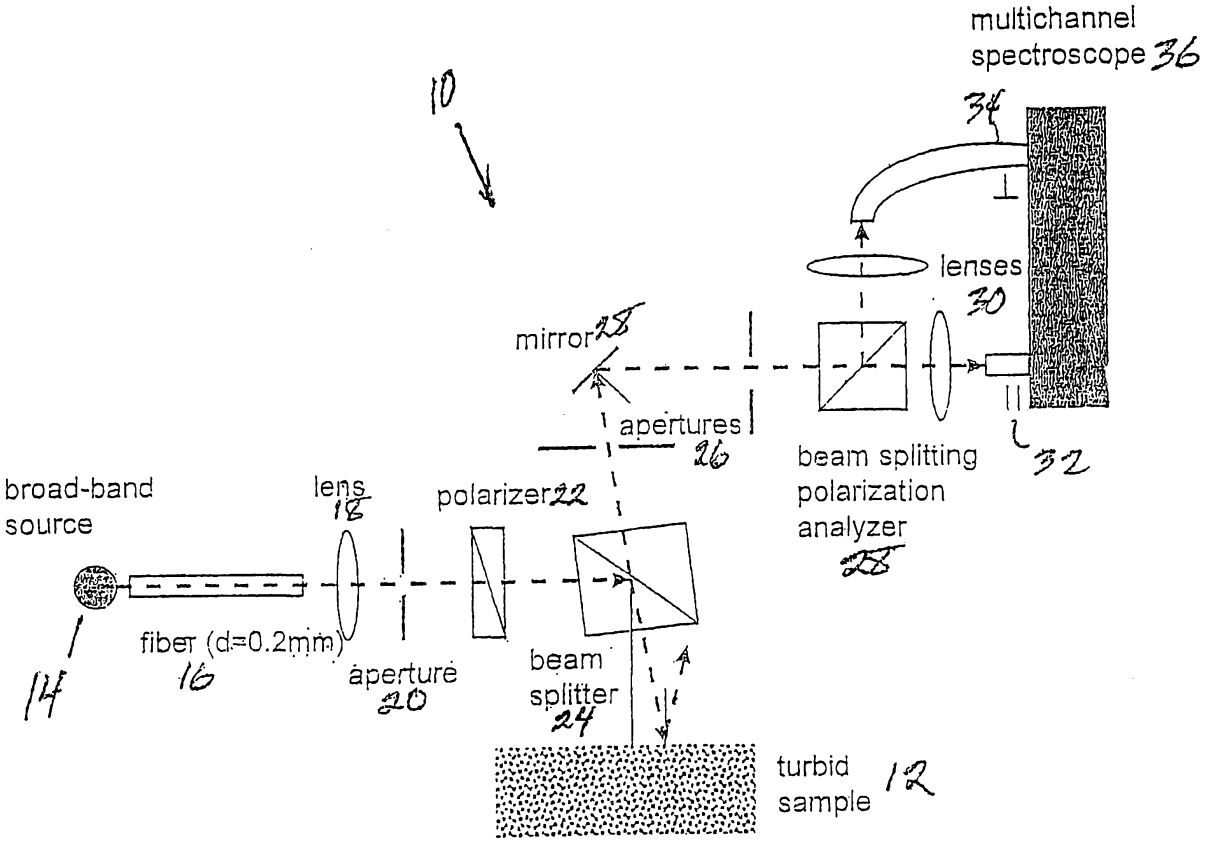
multichannel
spectroscope 36
10
34
lenses
30
mirror 28
apertures
26
beam splitting
polarization
analyzer
28
32
broad-band
source
lens
18
polarizer 22
fiber (d=0.2mm)
16
aperture
20
beam
splitter
24
14
turbid
sample
12

Figure 1

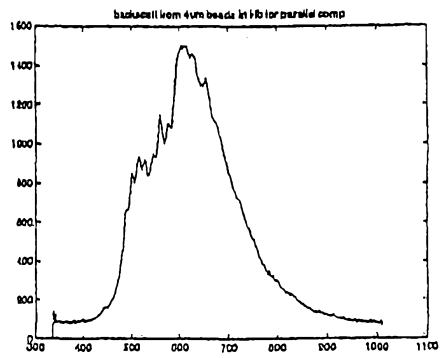

Figure 2A

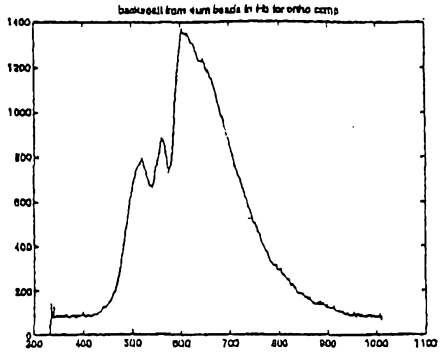

Figure 2B

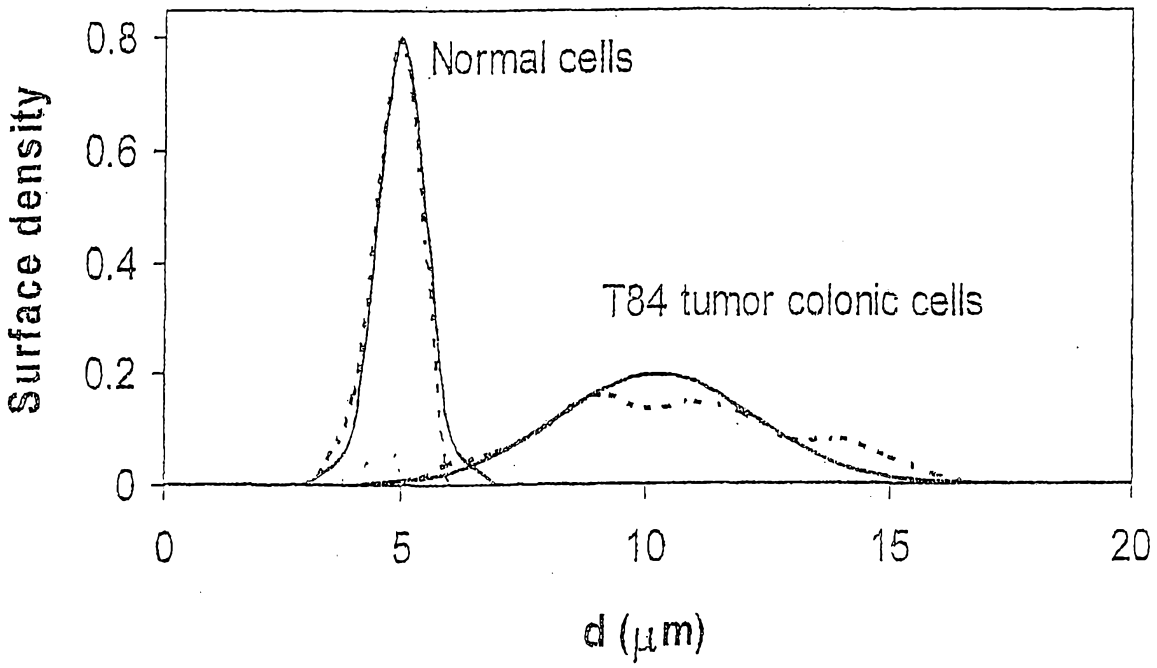

Figure 6

Figure 3A

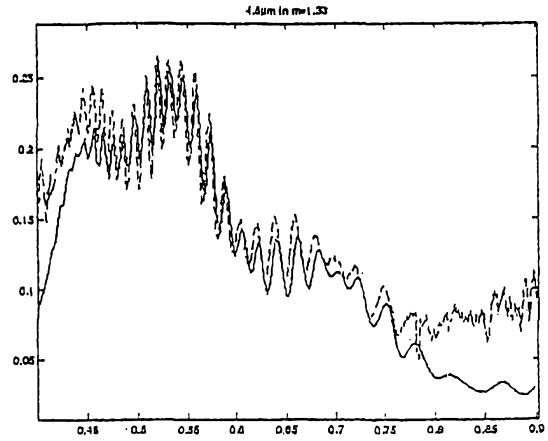

Figure 3B

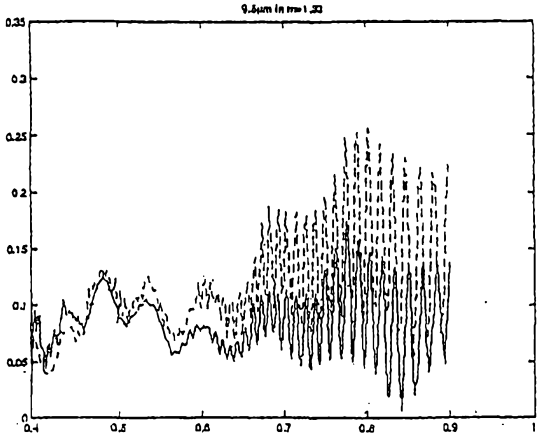

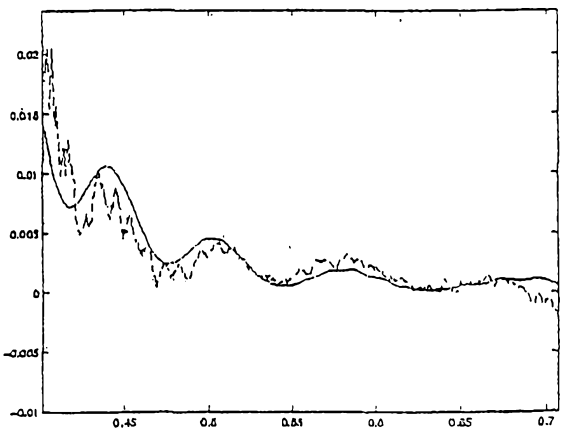

Figure 3C

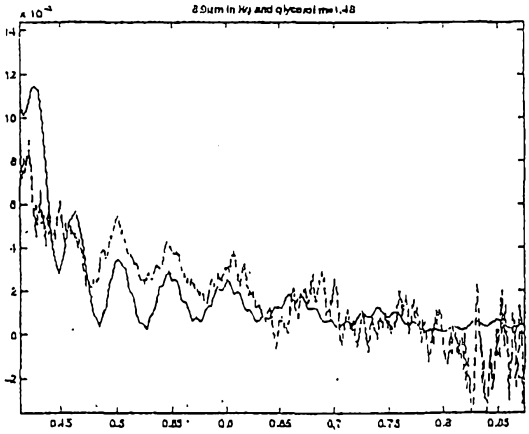

Figure 3D

Figure 4

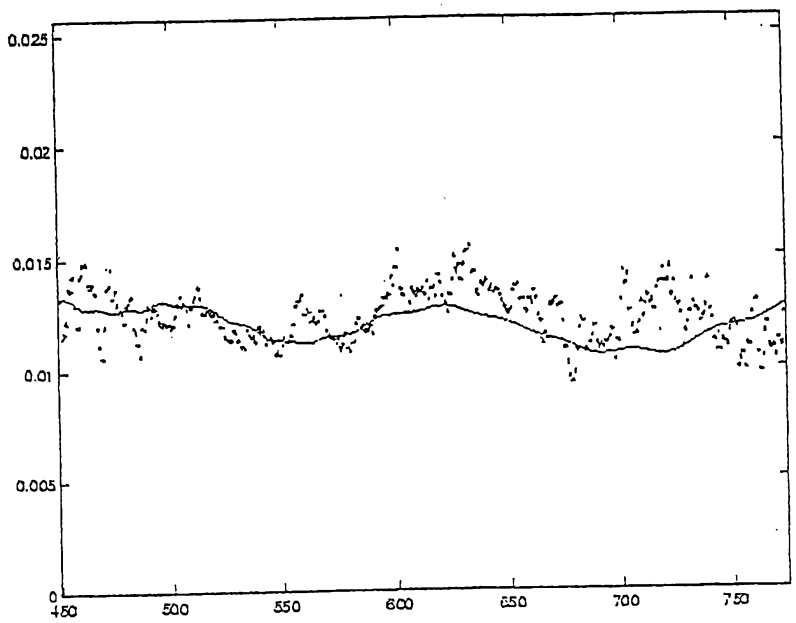

Figure 5

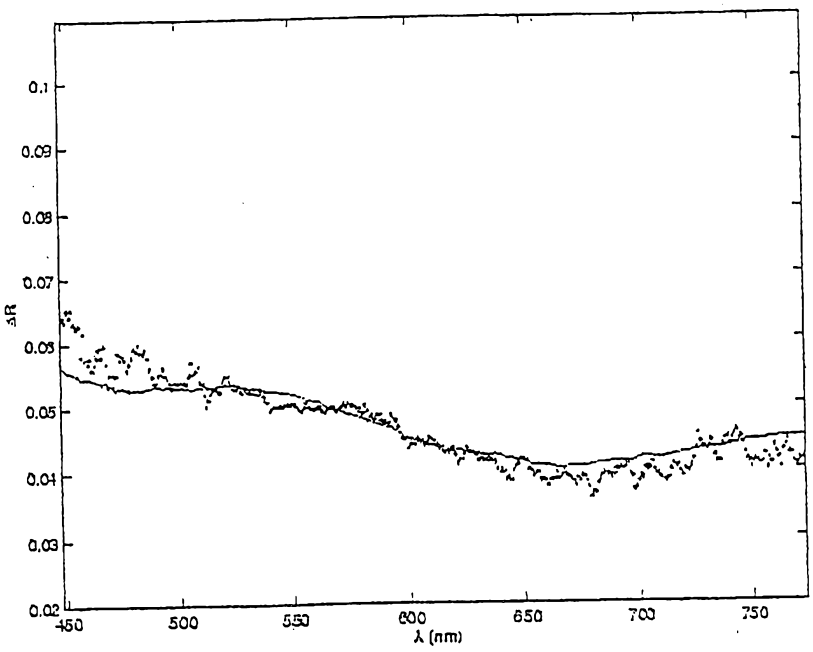

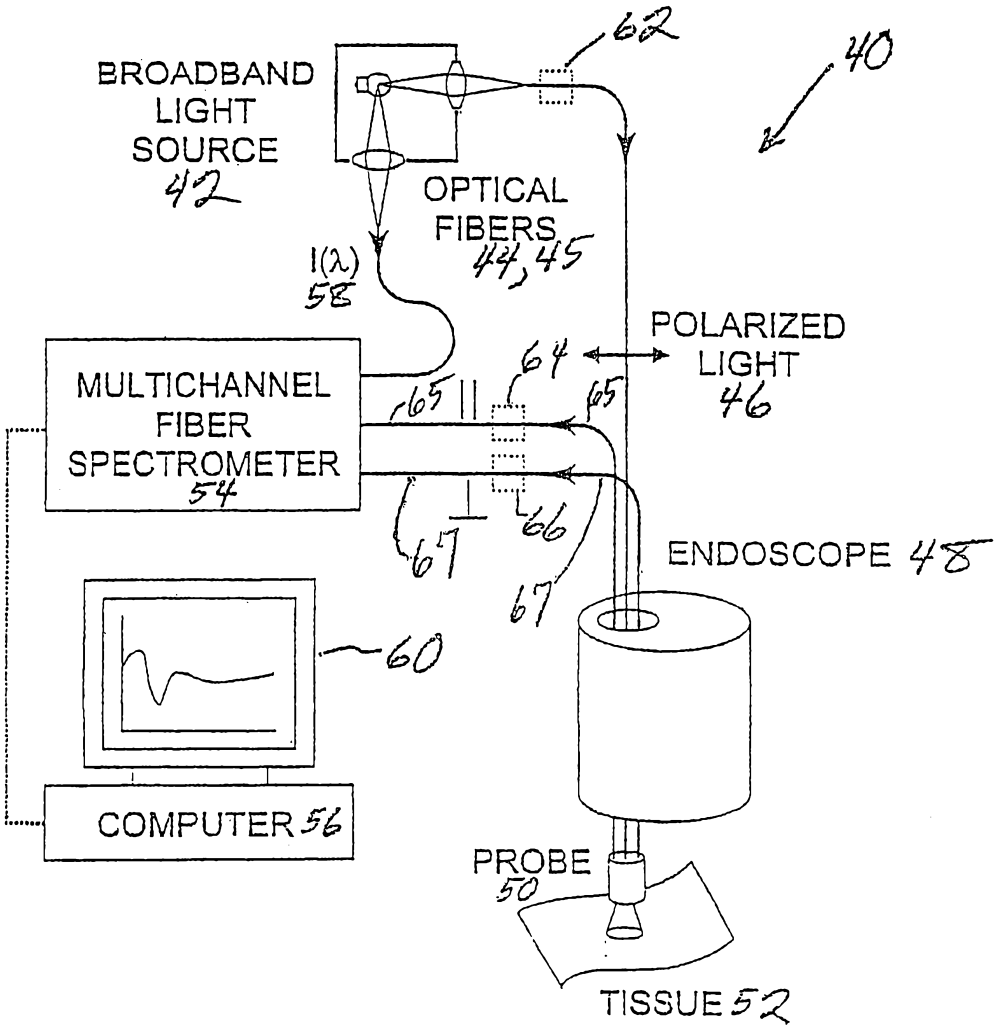
BROADBAND LIGHT SOURCE 42
62
40
OPTICAL FIBERS 44, 45
I(λ) 58
POLARIZED LIGHT 46
MULTICHANNEL FIBER SPECTROMETER 54
64
65
65
66
67
67
ENDOSCOPE 48
60
COMPUTER 56
PROBE 50
TISSUE 52

Figure 7

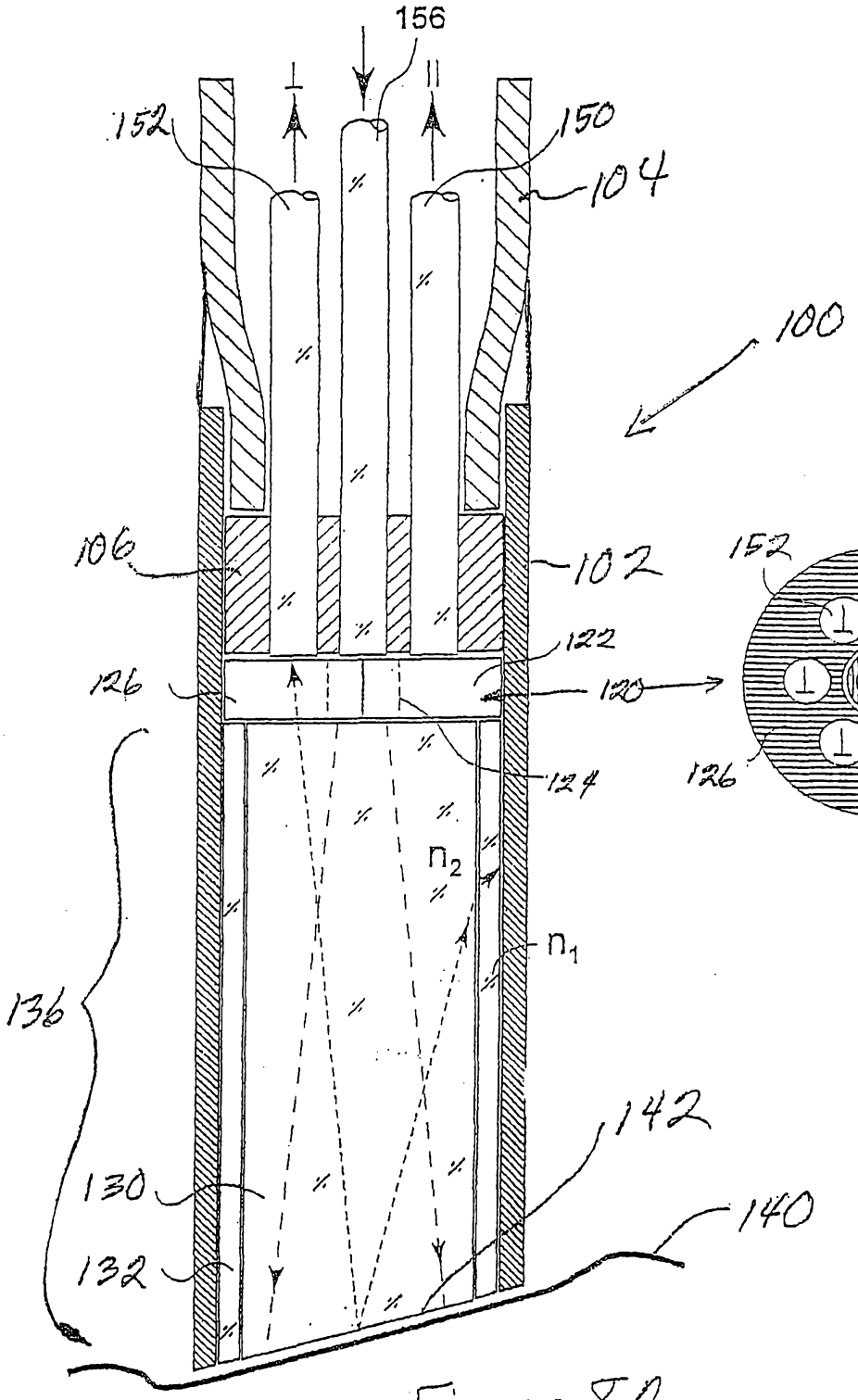

Figure 8A

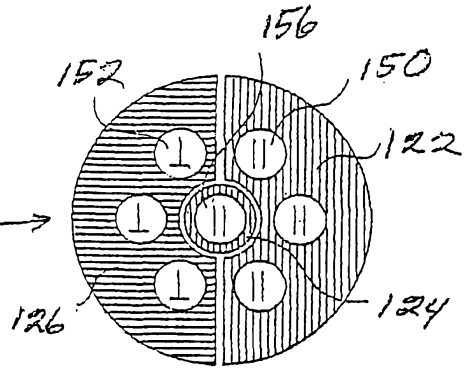

Figure 8B

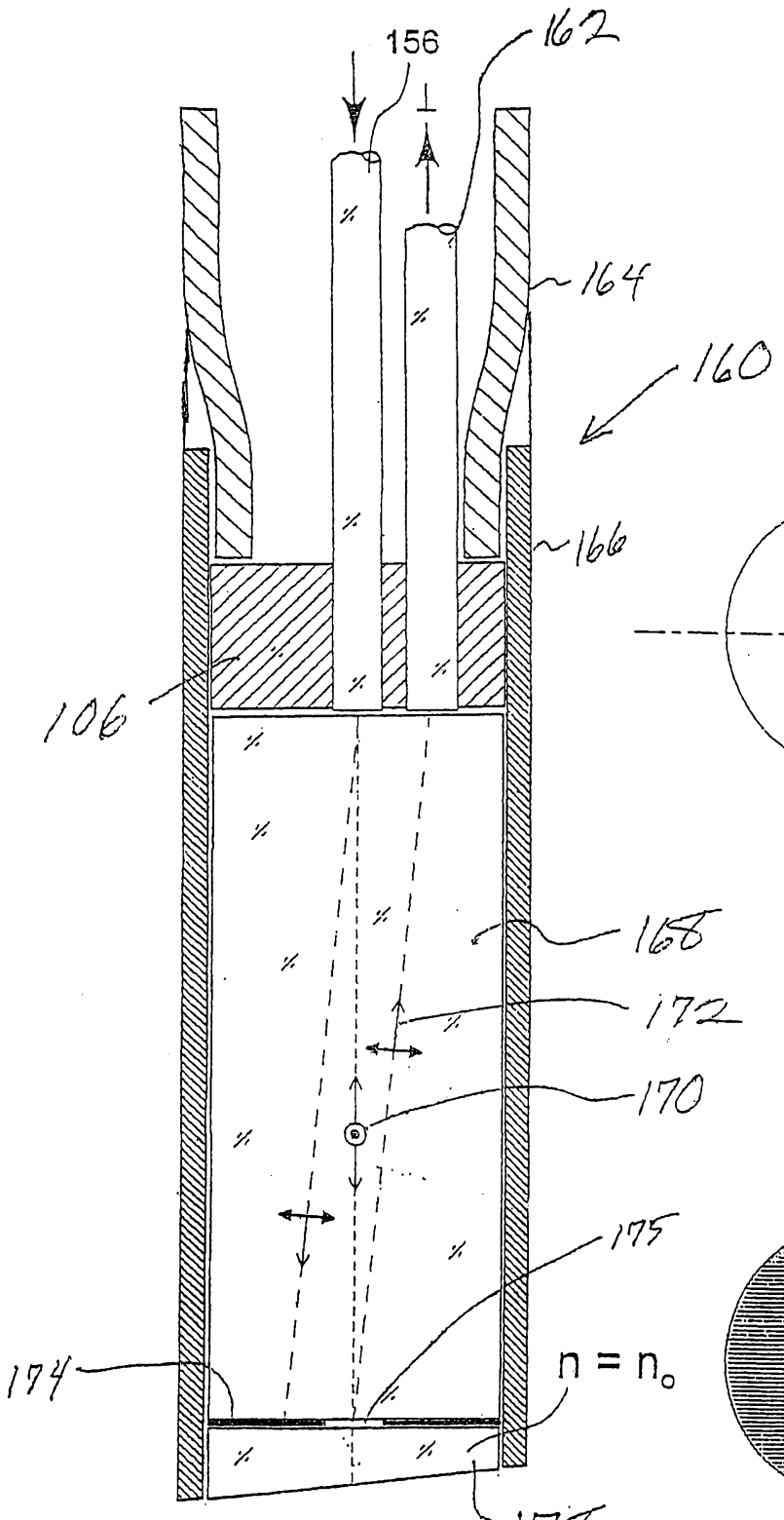

Figure 9A

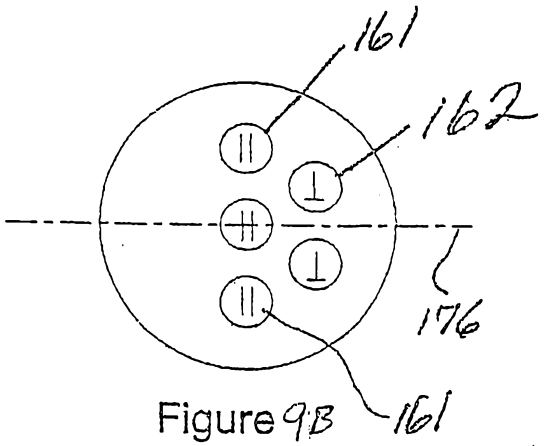

Figure 9B

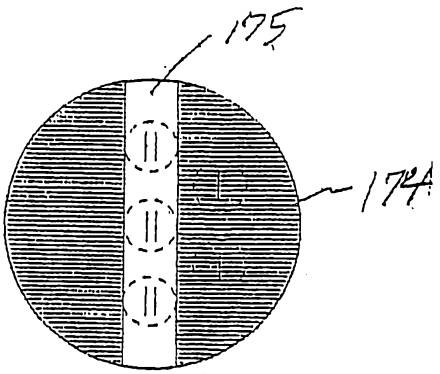

Figure 9C

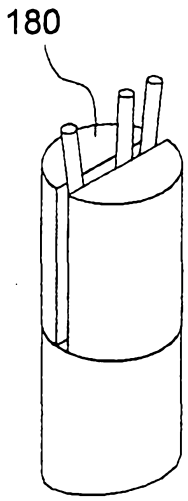

Figure 10A

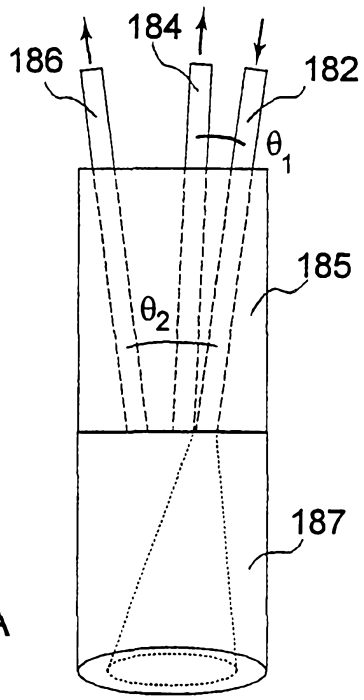

Figure 10B

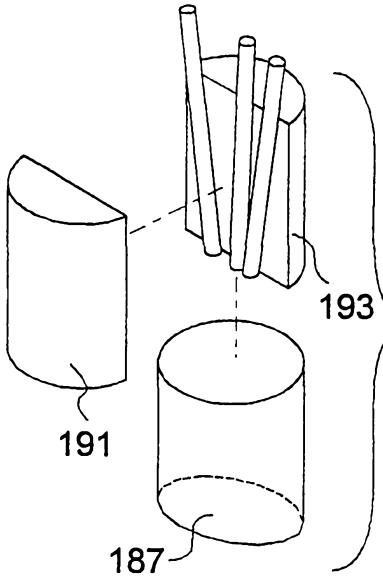

Figure 10C

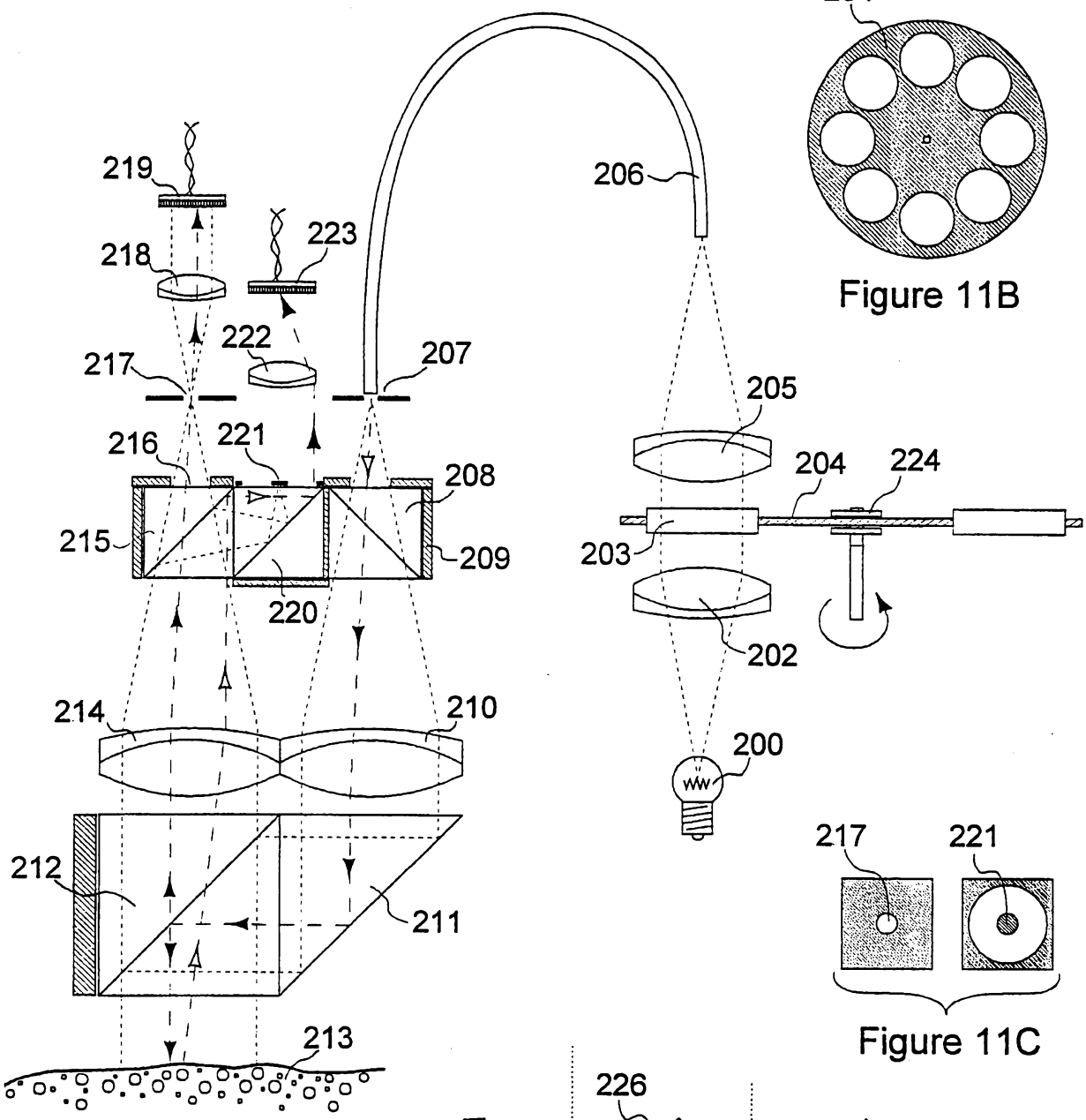

Figure 11A

Figure 11B

Figure 11C

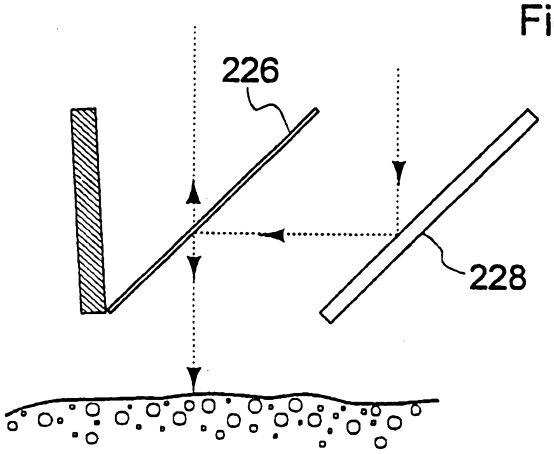

Figure 11D

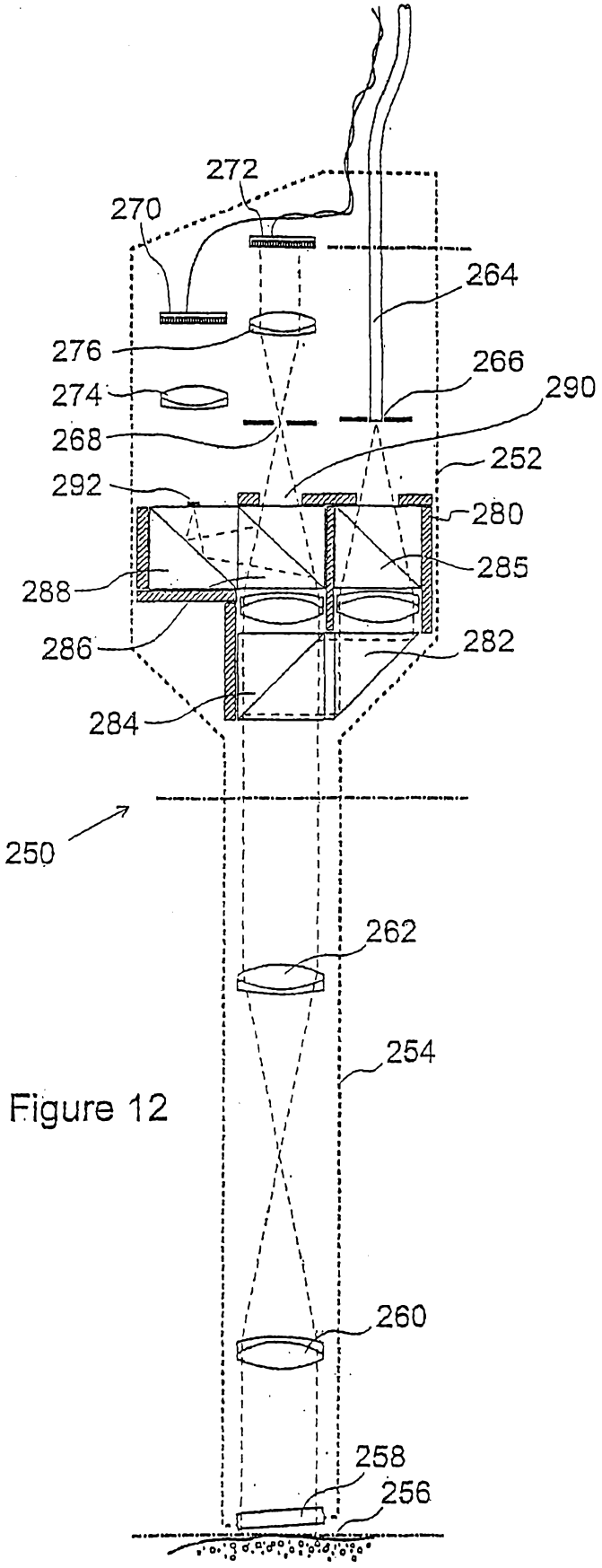
272
270
264
276
266
274
290
268
252
292
280
285
288
282
286
284
250
262
254
260
258
256

Figure 12

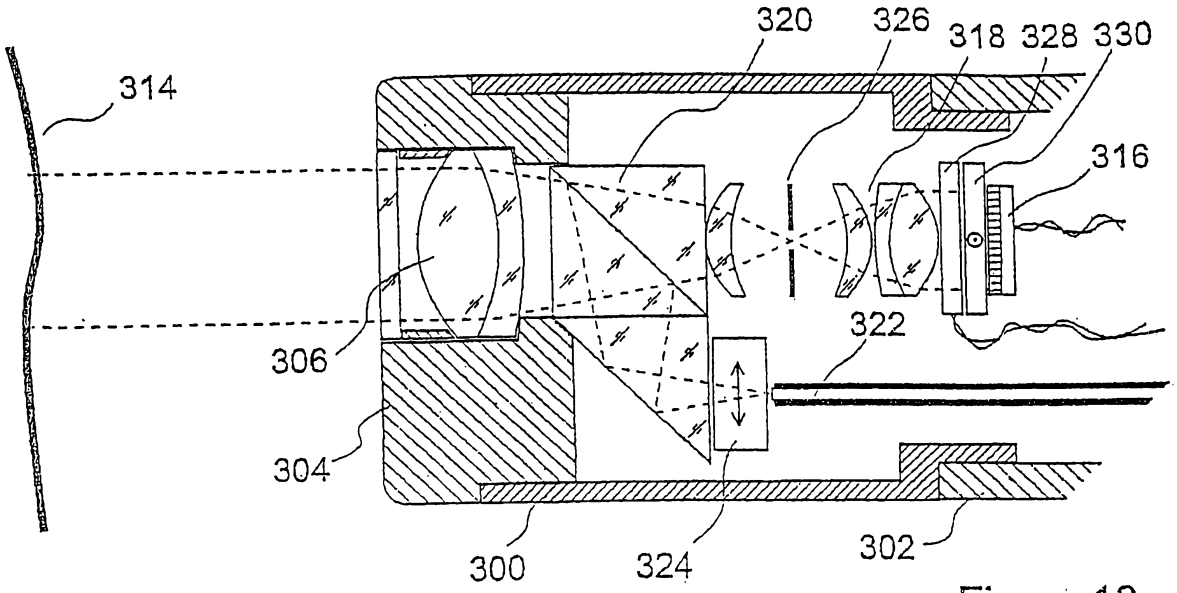

Figure 13

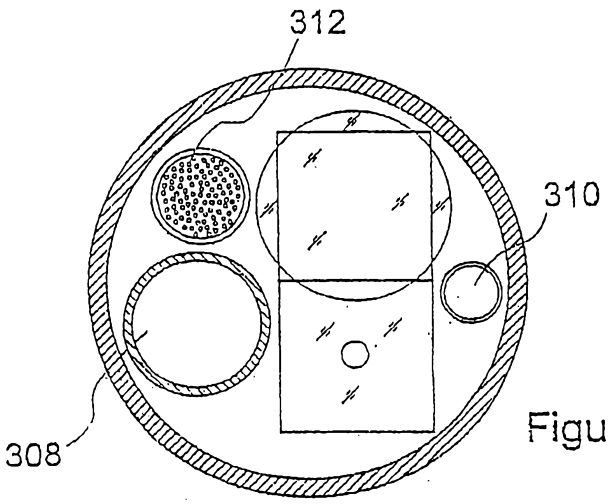

Figure 14

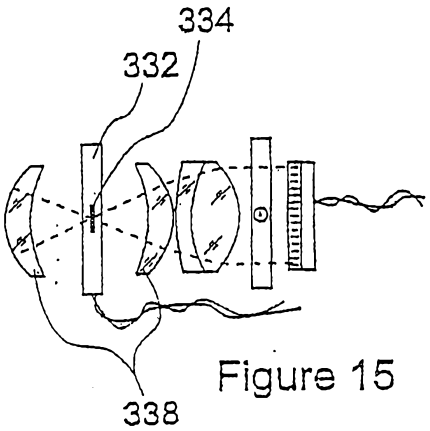

Figure 15

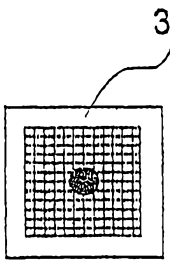

Figure 16

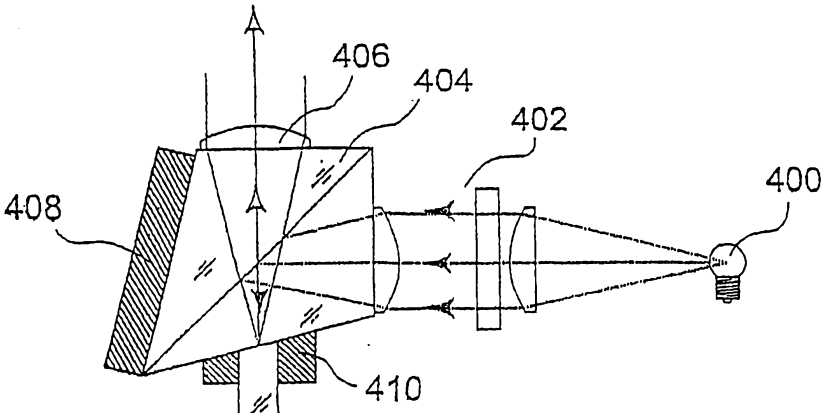

Figure 17

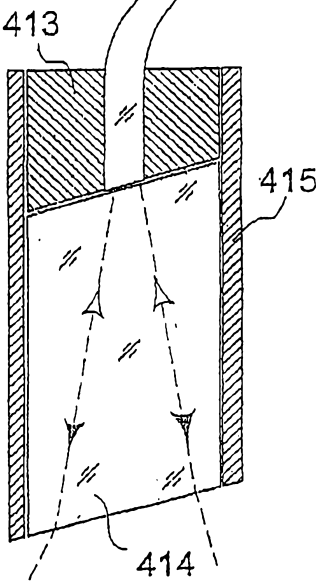

Figure 18

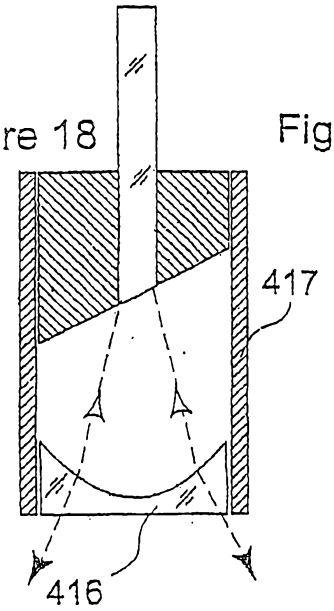

Figure 19

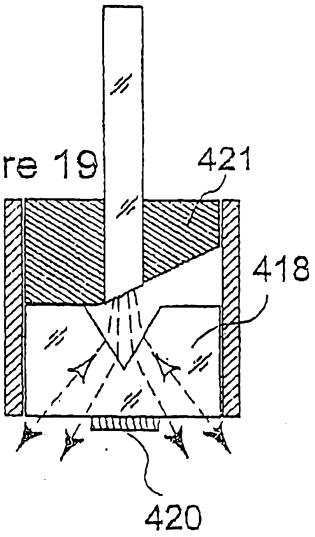

Figure 20

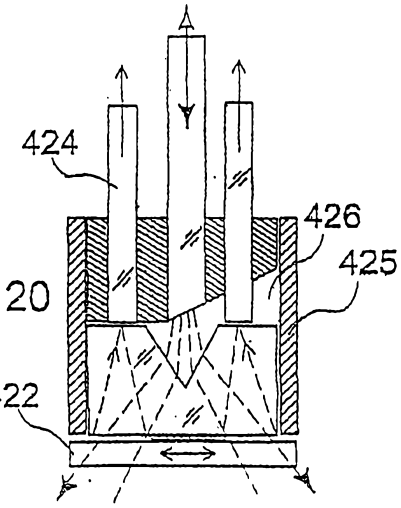

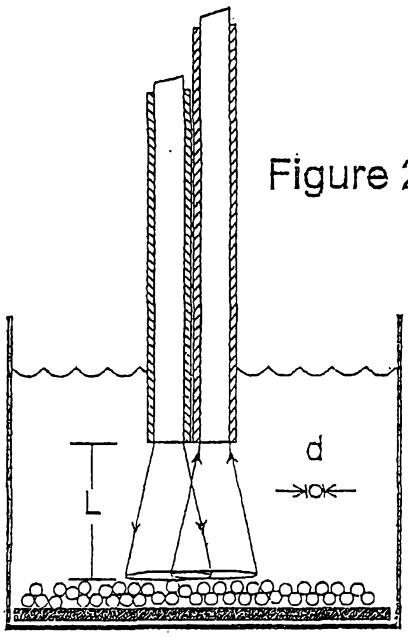

Figure 21A

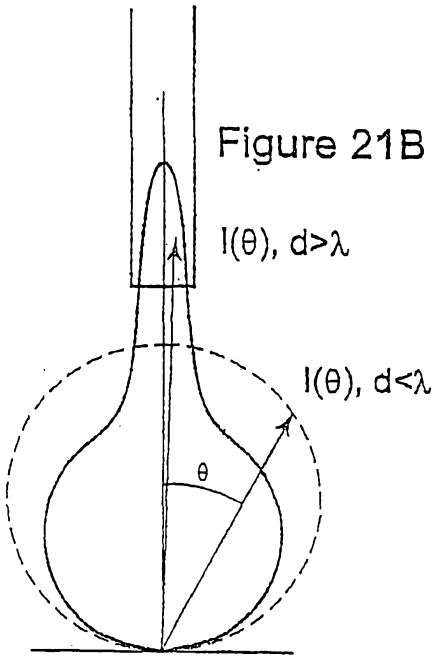

Figure 21B

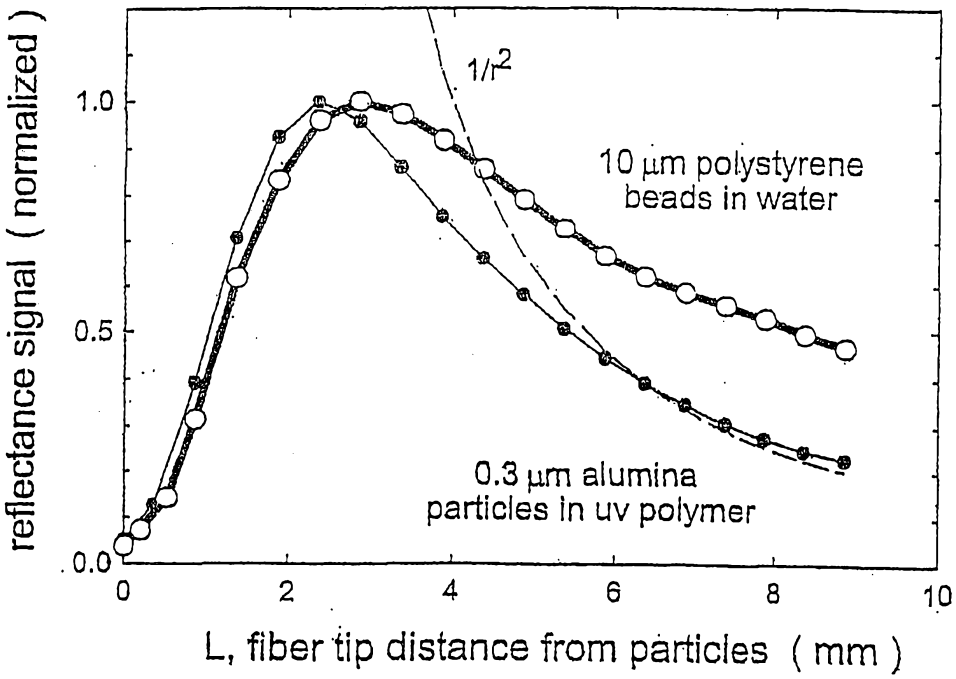

Figure 21C

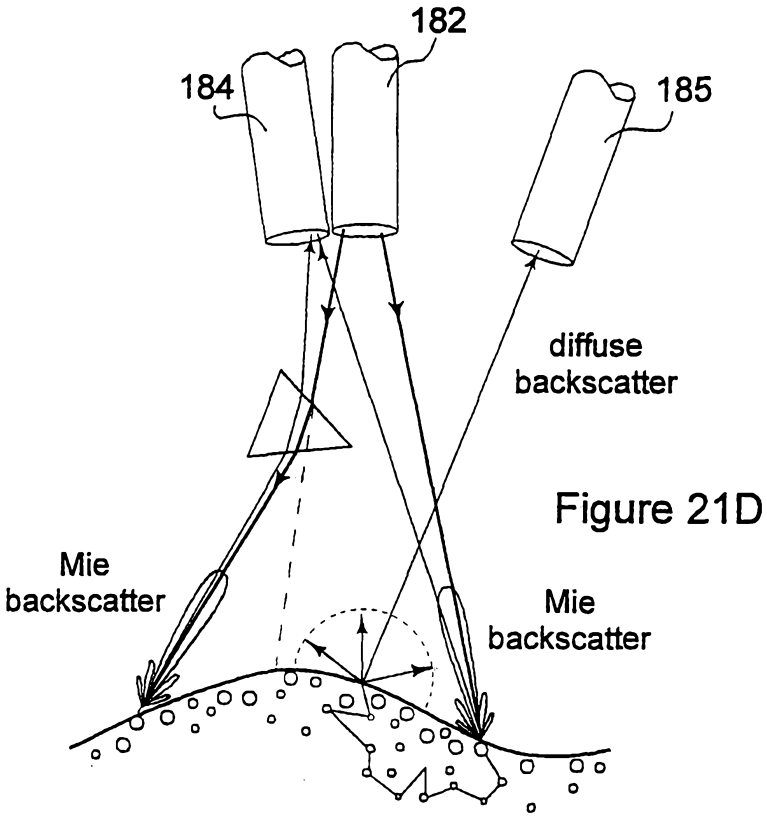
182
184
185
diffuse
backscatter
Mie
backscatter
Mie
backscatter

Figure 21D

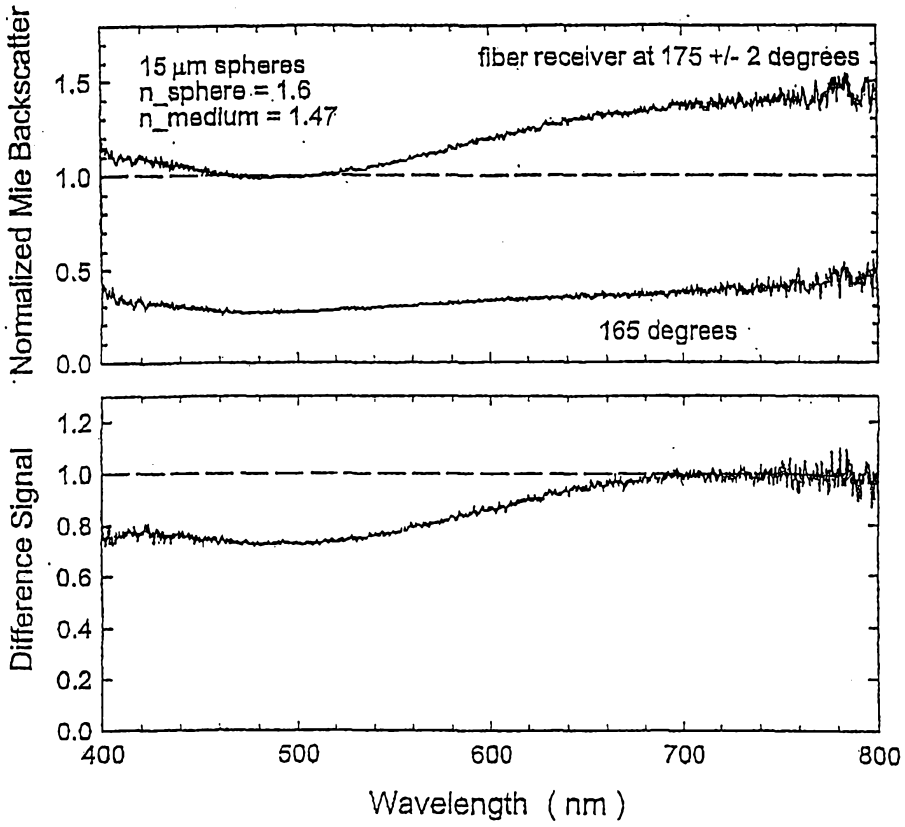

Figure 22A

Figure 22B